

A Guide to Computing Interfacial Properties of Fluids from Molecular Simulations [Article v1.0]

Erich A. Müller^{1*}, Åsmund Ervik^{2*}, Andrés Mejía^{3*}

¹Department of Chemical Engineering, Imperial College London, United Kingdom;

²Department of Gas Technology, SINTEF Energy Research, Trondheim, Norway;

³Departamento de Ingeniería Química, Universidad de Concepción, Chile

This LiveCoMS document is maintained online on GitHub at <https://github.com/asmunder/BPIPMDs>; to provide feedback, suggestions, or help improve it, please visit the GitHub repository and participate via the issue tracker.

This version dated March 8, 2021

Abstract Molecular simulation is ideally suited to explore and describe the behavior of inhomogeneous fluid mixtures as it allows a unique perspective into the physics at the scale relevant to interfacial properties, filling the gaps between experimental determinations and theoretical predictions. Although rather common Molecular Dynamics and Monte Carlo schemes are employed, the technical implementation and the post-processing of the results are more challenging than for homogeneous fluids due to the spatial dependence of the interfacial properties. This work is devoted to describing and recommending methods for molecular-simulation computation of the most important interfacial properties of pure fluids and fluid mixtures, *i.e.*, interfacial concentration of species, the interfacial thickness, the surface activity or adsorption of species, superficial enthalpy and entropy, wetting between phases and the interfacial or surface tension on planar interfaces. Herein, a detailed description is given of the steps required to perform classical molecular simulations including setting up of the initial configuration, choice of cell dimensions, thermodynamic conditions and ensemble, selection of the force field, simulation length, etc. and a discussion of the required post-processing steps in order to obtain interfacial properties. Additionally, general background and description of the expected results of interfacial fluid properties are provided, and step-by-step examples are included for the case of interfacial properties of pure fluids (carbon dioxide, decane) and mixtures (carbon dioxide + decane).

***For correspondence:**

e.muller@imperial.ac.uk (EAM); asmund.ervik@sintef.no (ÅE); amejia@udec.cl (AM)

1 Introduction

The term "interfacial properties" refers to the fundamental thermophysical properties that govern the behaviour of inhomogeneous fluids. The defining attribute of these systems is the existence of a boundary or interface, spanning only a few nanometers, but across which there are typically large changes in the local conformation of the fluids. The presence of this boundary region plays a central role in natural, environ-

mental, and industrial processes. The most representative of these interfacial properties are the concentration profiles of the species across the interface, the actual extent (thickness) of the interfacial region, the surface activity or adsorption of species at the interface, the superficial enthalpy and entropy, the wetting between phases, and last, but not least, the interfacial or surface tension. Some of these properties can be directly measured (*e.g.*, interfacial thickness, wetting

and interfacial/surface tension) [1] whereas others must be inferred from direct measurements, albeit usually with a high level of accuracy.

Molecular theories for interfacial properties are well developed, usually based on classical density functional theory [2–6], including the van der Waals square gradient theory [6, 7]. These theories have been shown to provide accurate results for both simple and complex mixtures, and their results are directly compare to molecular simulations can also share the same molecular parameters, [8–13] but inevitably some mixtures need extraneous information regarding interfacial properties to be effectively used as correlation tools.

On the other hand, molecular simulation is particularly well posed to study physical phenomena at the fluid interfaces. In these scenarios, while the perturbations caused by the fluid heterogeneities typically extend for several nanometers, rarely do the correlations in the neighbouring bulk phase fluid span distances larger than 50 nm. These are the system sizes which we are comfortable simulating with commonly available modern computers (and clearly this will only improve with time). This accessibility of the size and length scales pertinent to fluid interfaces has spawned in the recent past decades a surge in studies on the computational aspects of the interfacial tensions of pure fluids and mixtures, including the effects of third players (surfactants, nanoparticles, etc.)

The interfacial tension is typically not affected by the dynamics nor the prior history of the system¹, [6], hence it is amenable to be computed on the basis of an ensemble average of appropriate configurations. Both Molecular Dynamics (MD) [15] and Monte Carlo (MC) [16] methods can be employed with equal success to generate these configurations and this review makes little distinction between both strategies, as the tensions are calculated post-simulation by making suitable calculations on these configurations. MD has been used more extensively than MC in recent years, as MD has benefitted from advances in parallel computing and the use of graphical processing units [17].

The main advantage of classical molecular simulation (MS) for studying interfacial fluids is the explicit representation of the molecules in an environment which is commensurate with the dimension of the interfacial region of fluids ($\simeq 10$ to 100 \AA). The interfacial regions are characterized by sharp changes in densities and compositions, and these have to be considered explicitly, hence the overall system sizes in terms of number of particles can easily reach $O(10^5)$, or even $O(10^6)$ in cases with surfactants or proteins, which is considerably more than

¹The term “dynamic” interfacial tension refers to the scenarios where the tension changes with the observation time. These are not equilibrium conditions, but rather situations where the properties of the interfacial region are continually evolving, typically due to the slow mass transfer to/from the interfacial region of a third component, e.g., a surfactant. We will not be covering these aspects in this manuscript. See for example Dukhin et al. [14].

what is typical in single phase studies. Notwithstanding, the increasing power of computers and the improvement in speed of the available MS packages mean that evermore, this region of matter can be studied with increased scrutiny. Starting with the seminal publications on MS of interfacial properties from the middle of '70s [18], several authors have included in their manuscripts guidelines for obtaining meaningful calculations. However, these guidelines are dispersed and sometimes differ from author to author. The main goal of this manuscript is to provide a general, self-contained and unified guide to perform a MS for calculating interfacial properties of fluids using MD or MC. We do this by carrying out an exemplary MS of an inhomogeneous fluid detailing the advice with regards to the set-up, running and data analysis. In this work, we are focused on MS for computing interfacial properties of pure fluids and fluid mixtures in vapor-liquid equilibrium with planar interfaces.

The practices and methodologies described in this work can be applied for the cases of other planar fluid interfaces arising in liquid-liquid [19–23] and vapor-liquid-liquid equilibria [20, 24, 25]. For the case of curved interfaces, the reader is redirected to Refs. [6, 26–29].

2 Prerequisites

2.1 Recommended Reading

In addition to the recommendations, highlights and other issues concerning the prediction of interfacial properties are described in this document; we recommend the following textbooks and selected reviews and regular articles in this field.

- Allen and Tildesley, *Computer simulation of liquids*, 2^{ed}. pages 84–89 and Chap. 14. [15]

In this new edition of a classical textbook, the authors have included a chapter devoted to summarizing the most important aspects of carrying out MD and MC for inhomogeneous systems.

- Gray, Gubbins, and Joslin, *Theory of molecular fluids: Vol. 2: Applications*, Chap. 8. [30]

This book lucidly presents the principal elements of the statistical mechanics involved in the prediction of interfacial properties from MS, such as the Kirkwood pressure tensor and Test Area method.

- Ghoufi et al., *Computer modelling of the surface tension of the gas-liquid and liquid-liquid interface*. [31]

In this recent review the interfacial tension and related properties are calculated by using different methodologies using both MC and MD. A significant number of key references as well as previous reviews are listed within.

- Holcomb et al., *A critical study of the simulation of the liquid-vapour interface of a Lennard-Jones fluid*. [32]

This is a seminal paper where the implementation and use of Kirkwood pressure tensor to calculate interfacial tension is described. Still relevant today, this work summarizes some important issues concerning to the impact of the initial condition on the results from Kirkwood pressure tensor.

- Gloor et al., *Test-area simulation method for the direct determination of the interfacial tension of systems with continuous or discontinuous potentials*. [33]

This manuscript presented an alternative methodology to compute interfacial tension from perturbation theory rather than the more commonly used Kirkwood pressure tensor.

- Zhang et al., *Computer simulation of liquid/liquid interfaces. I. Theory and application to octane/water*. [34]

This work enumerates and comments on the several types of molecular ensembles available to carry out MS of interfacial tensions.

- Ervik et al. [35] and Sega et al. [36]

These works provide details and frameworks to carry out MD of fluid systems with interfaces, including post-processing, using Python codes.

- Additionally, references [37–44] are a few selected articles where the calculation of interfacial density (or concentration) and interfacial tension for pure fluids and fluid mixtures are described with emphasis on either methodology or reference fluid results.
- Finally, the reader is directed towards several publications that describe in detail the general aspects of molecular simulation:

- Braun et al., *Best Practices for Foundations in Molecular Simulations* [45]
- Bopp et al., *The Hitchhiker's Guide to Molecular Dynamics* [46]
- Grossfield et al., *Best Practices for Quantification of Uncertainty and Sampling Quality in Molecular Simulations* [47].

2.2 Software

There is a spectrum of molecular simulation packages to carry out molecular simulations of inhomogeneous fluids, ranging from commercial and academic versions to homemade codes. Most of them have a built-in subroutine to calculate the density or concentration along the interfacial region but rarely is there built-in provision to calculate interfacial/surface tension. This interfacial property should be calculated by modifying the original code or computed in a post-processing step as will be described later. Table 1 summarizes some examples of the molecular simulation packages frequently employed in academia for describing interfacial properties of fluids. In

general terms, MD software is available in parallelized versions, capable of running on multiple CPUs (and/or multiple GPUs) whereas MC software is normally only available in serial versions. The corresponding websites of these simulation packages typically include the user manual, some examples of the input files and output files as well as some benchmarks. The reader is redirected to Ref. [48] for a general classification of MS software.

Table 1. Summary of selected software to perform molecular simulations of inhomogeneous fluids. Checks (crosses) indicate the availability (unavailability) of provisions to output the density profile $\rho(z)$, interfacial tension γ , the ensemble average of the pressure tensor $\langle P_{kk} \rangle$ and/or the ensemble average of the pressure tensor in each slab along the z coordinate $\langle P_{kk}(z) \rangle$.

Software	Language	MS	$\rho(z)$	γ	$\langle P_{kk} \rangle$	$\langle P_{kk}(z) \rangle$
DL_POLY	Fortran	MD	✓	✗	✓	✗
GROMACS	C++	MD	✓	✓	✓	✗
HOOMD	C++	MD	✗	✗	✓	✗
LAMMPS	C	MD	✓	✓	✓	✓
NAMD	C++	MD	✓	✗	✓	✗
Gibbs ²	Fortran	MC	✓	✓	✓	✓

The selection of a simulation package is to some extent a personal decision, influenced by the general environment (*i.e.*, available support) and familiarity. For most simulations described here, the programs have been tested, validated and debugged as it is described on the corresponding websites of the softwares and the references therein (see however Sec. 7.5). For research applications it is well advisable to select a program written in a language which is familiar to the user, as most likely some level of modification will eventually be needed. In this regard, and with no prejudice, DL_POLY is an exemplary choice as its codes are written in a clear, modular, style providing for a reasonably straightforward way to implement additional subroutines. Speed of execution is also an important consideration, and there can be significant differences between the different compiled programs. In addition to calculation software, MS typically uses extra programs for three purposes: to setup initial configurations (*i.e.*, molecular editor), to plot resulting tabular data like such as time evolution of temperature and pressure, and to visualize spatial configurations and their temporal evolution. Some selected examples are the Avogadro [49], xmgrace [50], VMD [51], Ovito [52], and PyMOL [53] softwares. Avogadro is a molecular editor and visualizer which can be used to build initial configurations or to read molecular configurations in a myriad of styles, including the NIST webbook [54]. xmgrace is a 2D graphic software with high capability to easily read,

²The Gibbs program is commercially available as part of the Materials Design software suite <https://www.materialsdesign.com>

manipulate data, compute preliminary results and plot the output files from MS. VMD, Ovito and PyMol are 3D visualization programs useful to produce snapshots of spatial configurations and to visualize their temporal evolution. VMD, Ovito and PyMol can read numerous different file formats which making them very versatile. They also include some plugins to carry out some simpler calculations, such as computing and plotting density profiles. VMD and Ovito are free of charge software, whereas PyMol is a commercial software and requires an annual fee.

This guide discusses the background and details of molecular simulation for computing interfacial properties over the next six sections. A checklist for performing simulations is given in Appendix A.

3 General description and main equations to compute interfacial properties of fluids.

The properties in the interfacial region are characterized by their spatial dependence. In molecular simulations, the interfacial region is generally described as a function of a unidimensional coordinate. For the case of planar interfaces, the selected coordinate is z which is perpendicular to the interfacial area, here xy . For the case of spherical interfaces, such as drops or bubbles, the interfacial region is generally described as a function of a radius.

In this section, we enumerate the most common interfacial properties and the expressions for the planar interfaces case. For a complete description of these expressions, the reader is redirected to Refs. [15, 30].

3.1 Density Profiles

Fig. 1 illustrates a typical density profile, $\rho(z)$, in the z direction (perpendicular to the interface plane) for a pure fluid in a state of vapor-liquid equilibrium. A characteristic feature is the constant density in the bulk regions of the liquid (L) and vapor (V) (*i.e.*, $\rho = \rho^L$ or ρ^V), and sharp, but continuous, changes along the interfacial regions.

For the case of mixtures, the interfacial concentration of each component can exhibit different patterns than those shown in Fig. 1, where a simple monotonous drift is seen in the concentration profile from a higher to a lower density. Two other possible cases are schematically shown in Figs. 2 (a) and (b). Fig. 2 (c) illustrates a typical example of a binary mixture (*e.g.*, $\text{CO}_2 + \text{C}_{10}\text{H}_{22}$ at 344.15 K) where the fluid with lower interfacial tension shows adsorption (*e.g.*, CO_2)

In Fig. 2 (a) and (b), the concentration profile displays a stationary point, which is a maximum (point A) or a minimum (point D) of the concentration with respect to position. Both points reflect what is referred to as *surface activity*. In general

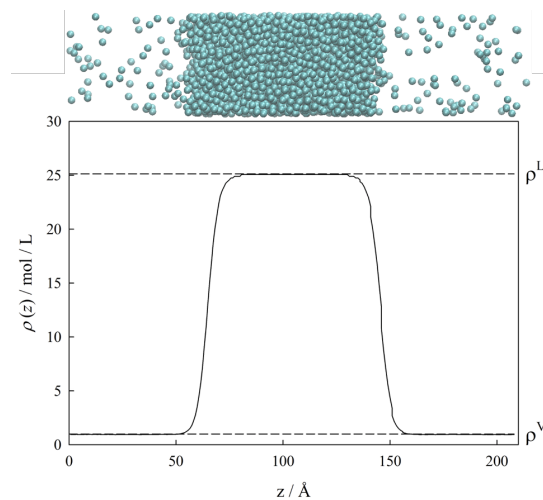


Figure 1. Density profile, ρ (black line) against the position coordinate perpendicular to the interface (z) for a pure liquid CO_2 in equilibrium with its vapor at 240 K. Overlaid is a snapshot of the detail of a simulation of a liquid-vapor interface.

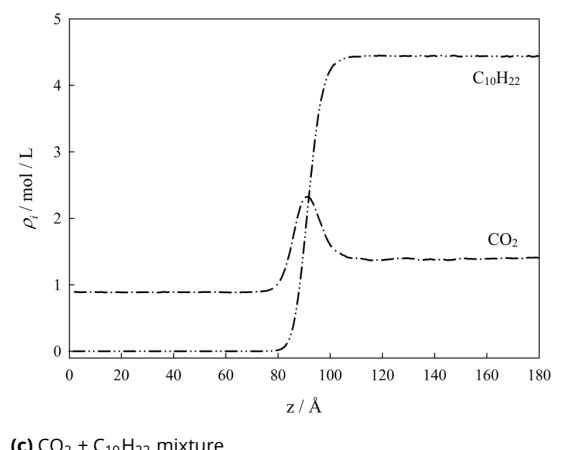
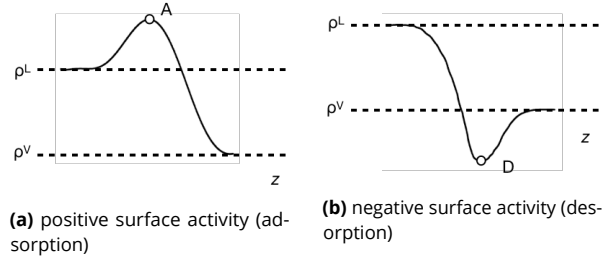


Figure 2. Concentration profiles in mixtures. (a) Schematic representation of positive surface activity (adsorption); (b) Schematic representation negative surface activity (desorption); (c) Density profile for the $\text{CO}_2 + \text{C}_{10}\text{H}_{22}$ mixture at 344.15 K and 2.39 MPa (cf. Example 2).

terms, surface activity refers to the accumulation (may it be positive or negative) of a species i at the interface region and is characterized by the condition, $d\rho_i/dz = 0$. The positive surface activity reflects absolute adsorption of species along the interface region and is reflected in a negative second derivative, $d^2\rho_i/dz^2 < 0$. Conversely, the negative surface activity denotes depletion of a species along the interface region, and its condition is given by $d^2\rho_i/dz^2 > 0$. As can be appreciated, a finite surface activity implies that the species reach higher (adsorption) or lower (desorption) concentrations than those seen in the bulk phases. In mixtures, the most common concentration profiles of species display no surface activity (component with high surface tension) or positive surface activity (component with low surface tension) [55]. Concentration profiles of species with negative surface activity have never been observed in experiments, but are predicted by some theories e.g. for mixtures with molar isopycnicity (or molar density) inversion [56] and for aqueous solutions of alcohols in liquid-liquid equilibria [19].

Surface activity will be described later by using the traditional Gibbs adsorption theory. Additionally, Fig. 2 (c) shows the concentration profiles for the case of the $\text{CO}_2 + \text{C}_{10}\text{H}_{22}$ mixture. In this case, the CO_2 exhibits adsorption, where the interfacial concentration of CO_2 is higher in the interfacial zone than bulk concentration. This behavior is common in mixtures for the component that exhibits the lower interfacial tension. In addition to the average density profiles previously described, the interfacial region is characterized by intrinsic density profiles caused by capillary wave fluctuations, which provide a route to carry out the detailed analysis of the interfacial structure. For a complete description and methodological approach, the reader is redirected to Bresme et al. [57, 58]. Since those works and references therein provide a thorough coverage of fluctuating interfaces, this work will not discuss the topic in further detail.

3.2 Interfacial Tensions

The interfacial (or surface) tension, γ , is arguably the best known and most widely studied of the interfacial properties. Strictly speaking, the term interfacial tension applies in any situation where two regions in space with different composition and/or state are separated by a clearly defined interface (e.g. solid/fluid, solid/solid, fluid/fluid). Many authors let interfacial tension refer specifically to liquid-liquid interfaces, and let surface tension refer to gas-liquid interfaces that may be a liquid in contact with its own vapor phase, or with a general gas such as air. In the context of this manuscript, the methods and discussion are more general, and so we do not make this distinction but use the terms interchangeably.

In MS, the interfacial (or surface) tension of pure fluids and fluid mixtures can be typically calculated from two different

approaches, namely a) the mechanical or pressure approach and b) the thermodynamic or perturbation approach.

For an inhomogeneous fluid, the pressure is a second-order tensor \mathbf{P} , where each component P_{ij} gives the force per unit area in the j -direction on a surface pointing in the i -direction. The axial symmetry about the z -axis (normal to the interface) and translational symmetry in the xy -plane imply that all the off-diagonal components are zero, thus there are only two independent, non-zero components: $P_{xx} = P_{yy} = P_T$, the tangential pressure (which changes along the interfacial region in the z direction); and the normal, or bulk pressure $P_N = P_{zz} = P$ which remains constant throughout the system, guaranteeing mechanical equilibrium. In the pressure approach, the interfacial (or surface) tension, γ , is given by the Hulshof integral [59], which is based on evaluating the inhomogeneity of the pressure tensor:

$$\gamma = \int_{-\infty}^{+\infty} [P_N - P_T] dz \quad (1)$$

An alternative, but equally rigorous approach, recognizes that the interfacial (or surface) tension may be expressed statistically as the difference in free energy for systems in closely related macrostates with different interfacial areas. In this so-called thermodynamic approach, γ is calculated from the following expression [30, 33, 43]:

$$\gamma = \left(\frac{\partial F}{\partial A} \right)_{N, T, V} \quad (2)$$

Where F is the Helmholtz free energy of the system³. The derivative is calculated by performing an (almost) infinitesimal perturbation in the interfacial area A at canonical conditions (keeping the compositions, volume V and temperature T of the system constant). The details of the implementation of these methods is the subject of Sec. 5.

Fig. 3 illustrates some examples of the experimentally observed behaviour of γ in pure fluids and fluid mixtures. For the case of pure fluids and zeotropic fluid mixtures in vapor-liquid equilibrium (the most common scenarios), γ decreases as temperature or pressure increases. A similar monotonous decay can be observed with changing compositions. For the case of azeotropic [$(\partial P/\partial x_i) = 0$ or $(\partial T/\partial x_i) = 0$] or aenotropic [$(\partial \gamma/\partial x_i) = 0$] fluid mixtures, γ exhibits a stationary point [$(\partial \gamma/\partial x_i) = 0$; $(\partial \gamma/\partial P) = 0$; $(\partial \gamma/\partial T) = 0$]. These stationary points reflect a change of the surface activity of species i . These are infrequently encountered systems and conditions, normally associated with certain pathological types of liquid-liquid equilibria, where γ shows a parabolic behaviour with temperature or pressure.

³Most commonly in the engineering literature the Helmholtz free energy is symbolized by the letter "A". However, in the context of this manuscript this would lead to a confusion between this quantity and the surface area, which we label herein as "A".

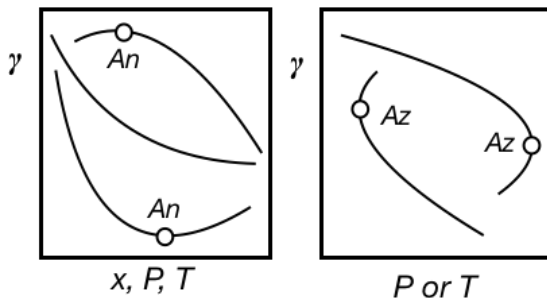


Figure 3. Schematic examples of the possible behaviour of the interfacial (or surface) tension (γ) with temperature (T), pressure (P) or mole fraction (x) in either vapor-liquid, or liquid-liquid equilibria. An refers to aneotropic points, Az refers to azeotropic points.

A third class of methods is based on the concepts of finite-size scaling within the grand canonical ensemble [60, 61]. Essentially, umbrella sampling is used to fully sample the relevant range of values for the number of particles N present in the grand canonical system, thus providing a free-energy density profile (which is directly related to the density profile) from where the interfacial density may be derived. The method is particularly suitable in the vicinity of the critical region where other methods are cumbersome to apply, but its implementation [15, 62] will not be discussed herein.

3.3 Derivative interfacial properties

The density (or concentration) profiles along the interfacial region, $\rho_i(z)$, and the interfacial (or surface) tension, γ , are by far the most reported of the thermophysical properties of fluid interfaces. Aside from their own inherent value, these properties provide a route to calculate others descriptors of the interface such as the interfacial thickness, δ , the relative Gibbs adsorption isotherm, Γ_{ij} , the change of surface entropy, s^γ , and surface enthalpy, h^γ , and the critical temperature of pure fluids, T_c , as we describe below.

3.3.1 The interfacial thickness

The interfacial thickness δ is defined as the width of the region where observable properties such as density change with the spatial coordinate. The range of the interfacial thickness typically oscillates between 10 to 200 Å at subcritical conditions and has an exponential increase with temperature. As the system tends to the critical state, the width diverges, $\delta \rightarrow \infty$. Clearly, as the continuous nature of the density (composition) variation precludes any unique definition of where the bulk region ends and where the interface itself dominates, some arbitrary criterion must be invoked. A popular choice is the so-called 10/90 criteria. Within this definition, δ represents the z range where the density profile changes from $\rho^\alpha + 0.1(\rho^\beta - \rho^\alpha)$ to $\rho^\alpha + 0.9(\rho^\beta - \rho^\alpha)$, where ρ^α and ρ^β are the bulk densities in the α and β phases, respectively.

For the case of pure fluid, δ can be calculated by fitting the following expression to the density profile[5, 6]:

$$\rho(z) = \frac{1}{2} (\rho^\alpha + \rho^\beta) - \frac{1}{2} (\rho^\alpha - \rho^\beta) \tanh \left[\frac{\theta(z - z_0)}{\delta} \right] \quad (3)$$

where ρ^α and ρ^β are the densities of the bulk phases with $\rho^\alpha > \rho^\beta$; z_0 is a reference coordinate, which is usually taken as the mean interface or the position of the Gibbs dividing surface (see next section) and $\theta = 2 \tanh^{-1} 0.8 = 2.19722$; this latter value chosen so that δ can be defined as the 10/90 interfacial thickness.

The use of the tanh (or equivalent fitting function such as erf) suggests that one could express the adsorption (or depletion) of a species as the difference between the pointwise composition (or density) and that of the bulk regions, as will be described in the next sections.

3.3.2 The relative Gibbs adsorption isotherm

The relative Gibbs adsorption isotherm of a species i relative to a species j (Γ_{ij}) can be thus defined in terms of $\rho_i(z)$ by the following integral equation [6]:

$$\Gamma_{ij} = \int_{-\infty}^{z_0^j} [\rho_j(z) - \rho_j^\alpha] dz + \int_{z_0^j}^{+\infty} [\rho_j(z) - \rho_j^\beta] dz \quad (4)$$

In Eq. 4, z_0^j is the transition point between the two bulk phases and corresponds to the position of the Gibbs dividing surface relative to a species j . z_0^j is calculated from Eq. 4 considering that species j does not have adsorption along the interfacial region, i.e., z_0^j is solved for the case that $\Gamma_{jj} = 0$. Mathematically, z_0^j is given by the expression:

$$z_0^j = \frac{\int_{-\infty}^{+\infty} \rho_j(z) dz}{\rho_j^\alpha - \rho_j^\beta} \quad (5)$$

Fig. 4 (a) illustrates this construction, which essentially maps the areas between the smooth density profile and a hypothetical infinitely steep (and thin) interface in such a way that the dividing surface corresponds to the average interface. If there is more than one component in the system, the Gibbs dividing surface for component j does not need to correspond a point of average null adsorption for other components. As seen in Fig. 4 (b), another component i in the mixture may display adsorption at the interface relative to a species j .

Alternatively, Γ_{ij} can be calculated from the expression proposed by Telo da Gama and Evans[63]:

$$\Gamma_{ij} = - \left(\rho_j^\beta - \rho_i^\alpha \right) \int_{-\infty}^{+\infty} \left\{ \frac{\rho_j(z) - \rho_j^\beta}{\rho_j^\beta - \rho_j^\alpha} - \frac{\rho_i(z) - \rho_i^\beta}{\rho_i^\beta - \rho_i^\alpha} \right\} dz \quad (6)$$

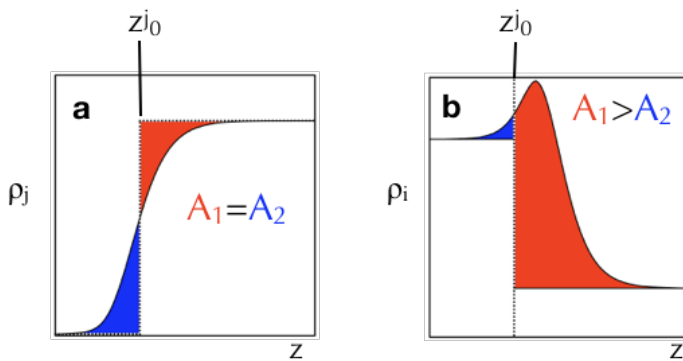


Figure 4. (a) Schematic position of the Gibbs dividing surface z_0^j calculated by selecting the point of no adsorption, $\Gamma_{jj} = 0$, where the areas above and below the density profile cancel out. (b) For other components i in the mixture, this Gibbs dividing surface suggests the adsorption of a species i , $\Gamma_{ii} > 0$.

3.3.3 The surface entropy and surface enthalpy

The entropy (s^γ) change of surface formation can be deduced from the Gibbs-Duhem expression for interfaces and the homogeneous first-order function of the interfacial tension (γ). Mathematically, the Gibbs-Duhem expression for interfaces is given by [6, 64]:

$$-d\gamma = s^\gamma dT - \tau^\gamma dP^\gamma + \sum_{k=1}^c \Gamma_k^\gamma d\mu_k^\gamma \quad (7)$$

where T is the temperature, t is the thickness of the surface, the superscript γ denotes interfaces, P is the pressure, c number of components, Γ_k and μ_k are the surface concentration and the chemical potential, respectively, for species k .

The interfacial tension, γ , can be also expressed as a homogeneous first-order function of the extensive parameters (T, P, μ_k) [6, 64]:

$$d\gamma = \left(\frac{\partial \gamma}{\partial T} \right)_{P, \mu_k} dT + \left(\frac{\partial \gamma}{\partial P} \right)_{T, \mu_k} dP + \sum_{k=1}^c \left(\frac{\partial \gamma}{\partial \mu_k} \right)_{T, P} d\mu_k \quad (8)$$

From Eq. 7 and 8, s^γ is calculated from the following expression:

$$s^\gamma = - \left(\frac{\partial \gamma}{\partial T} \right)_{P, \mu_k} \quad (9)$$

The enthalpy (h^γ) change of surface formation can be obtained from the fundamental equation of internal energy (u) with interfaces and its Euler associate expression. Mathematically, the fundamental equation is given by [6, 64]:

$$du^\gamma = Tds^\gamma - P^\gamma d\tau^\gamma + \gamma + \sum_{k=1}^c \mu_k^\gamma d\Gamma_k^\gamma \quad (10)$$

From Eq. 10, the enthalpy (h^γ) change of surface formation can be calculated as:

$$h^\gamma = \gamma + Ts^\gamma \quad (11)$$

These quantities cannot be directly measured, but are inferred from surface tension isotherms.

3.3.4 Critical temperature of a pure fluid

Although not strictly an interfacial property, the value of the critical temperature of a pure fluid, T_c , can be conveniently estimated by extrapolating the thermal evolution of the interfacial tension ($\gamma - T$) and employing scaling laws. For the case of γ , the following expression holds [6]

$$\gamma = \gamma_0 \left(1 - \frac{T}{T_c} \right)^{1.26} \quad (12)$$

where γ_0 and T_c are treated as unknown constants, and their values are found by fitting the interfacial tension data with temperature. The exponent in Eq. 12 corresponds to the Ising universality value, which is applicable to real fluids. There is however no guarantee that it can be applied to any general molecular force field.

4 Initial setup of the simulation

4.1 Shape of the simulation cell

The system sizes for the MS of interfacial systems are necessarily larger than their pure phase counterparts (or the vapor-liquid equilibrium if one considers Gibbs Ensemble MC simulations), as one must simultaneously track two bulk phases and two interfacial regions at the same time. In order to guarantee the simultaneous formation of two bulk phases (e.g., vapor and liquid or liquid and liquid) and the interfacial region, it is customary to use a rectangular parallelepiped simulation cell, where one Cartesian direction is larger than the other two. By employing this geometry, one forces the appearance of slabs of liquid and vapor (or liquid 2) sandwiched side by side. The system will spontaneously form the interfaces spanning the minimal area, parallel to the xy plane. The volume of the simulation box, V , is given by $L_x L_y L_z$, where $L_x = L_y$ and $L_z \gg L_x$. Due to the periodic boundary conditions, each bulk phase is bounded by two independent interfaces. The periodic boundary conditions in xy directions allow for conditions representative of essentially infinite interfaces. The use of small systems and/or cubic geometries risks the formation of bubbles/drops or similar bridges between clusters of molecules and their periodic images⁴.

⁴In some cases, this may actually be the desired outcome. For example in the study of the interfacial tension of drops and bubbles, relatively large cubic boxes are employed, where a drop/bubble forms far away from its periodic images. See for example [65]

Standard practice is to make the box large (and elongated), and several authors have studied in detail [66–68] the minimum dimensions for the simulation box. For the case of a parallelepiped cell ($L_x \times L_y \times L_z; L_z > L_x, L_y$), the interfacial area ($L_x \times L_y$) needs to be at least such that $L_x = L_y > 10$ times the molecular diameter (or bead diameter). This is to avoid oscillatory behavior of vapor pressure and surface tension due to finite size effects. L_z , in turn, needs to be 3 to 10 times L_x, L_y . These values are chosen with the purpose to accommodate enough molecules to ensure sensible-sized bulk phases and the corresponding two interfacial regions. In general terms, this route to define the cell dimensions are adequate for several types of pure fluid and fluid mixtures. However, for the case of long-chain molecules, it is advised to replace the bead size by the radius of gyration. The latter selection avoids the issue of molecules interacting with themselves.

4.2 Initial setup of the simulation cell

To perform the inhomogeneous simulation, one must place in the simulation cell both phases in intimate contact. A naïve and impractical way is to pre-equilibrate the coexisting phases at the approximate conditions of temperature, density and composition and build a composite box by joining both pre-equilibrated boxes. Although possible, this strategy is not trivial to implement, in particular when dealing with complex molecules, as the periodic boundary conditions must be unravelled and the interface region is prone to have overlaps between the cojoined boxes. There are two practical ways around this problem, the volume expansion or the temperature quench methods.

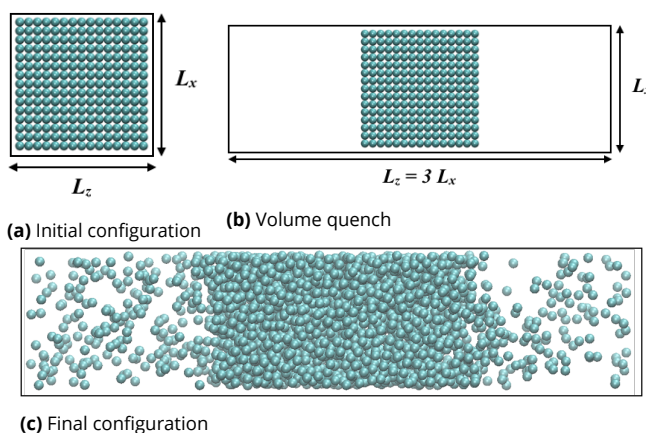


Figure 5. Initial configurations for the volume expansion method. (a) An initial cubic simulation box is set up with the density close to that of the expected liquid phase. Molecules may be in a lattice position, randomly placed or can be the output of an equilibrated pure fluid simulation. (b) The simulation box is expanded in the z direction, leaving empty spaces on both sides. (c) Upon further equilibration, some of the liquid phase molecules will evaporate, filling the void space until the vapor pressure is attained.

In the volume expansion (or volume quench [32]) case, an initial ensemble of molecules is placed, usually in a cubic periodic box, in a lattice configuration or randomly distributed within the simulation cell. The dimension of the simulation box can be set by specifying the number of molecules desired (see below) and the expected liquid density, whose value can be obtained from experimental data, molecular-based EoS, or other simulations using the same force field. Once the system equilibrates to the required temperature, two empty boxes are included at both z-sides, making the final dimension box equal to $L_x \times L_y \times (3 \text{ to } 10)L_x$. This procedure is illustrated in Fig. 5. A further equilibration will allow some of the liquid molecules to evaporate and fill the void regions until the equilibrium vapor pressure is attained. This technique is particularly suited for the case of vapor-liquid equilibria of single site molecules (spheres) at low temperatures.

EXAMPLE 1: Selection of simulation box size and number of particles for a volume expansion.

As an example, let us consider the MS for pure CO₂ at 240 K in the liquid state. For this case, CO₂ will be represented by a single sphere (Mie potential) of diameter of $\sigma = 3.741 \text{ \AA}$ [69]. We take a total of 3200 spheres and using the expected liquid density, $\rho = 24.742 \text{ mol/L}$ [54]:

$$\begin{aligned} V &= \frac{(3200 \text{ particles}) (10^{10})^3 (\text{\AA}/\text{m})^3}{24.742 (\text{mol}/\text{L}) (N_{\text{av}}) (\text{molecules}/\text{mol}) (1000) (\text{L}/\text{m}^3)} \\ &= 214770 \text{\AA}^3 \end{aligned} \quad (13)$$

where $N_{\text{av}} = 6.022 \cdot 10^{23}$ is Avogadro's constant. Using the value of the expected volume and a cubic cell, its vertex will be $L_x = \sqrt[3]{V} = 59.886 \text{ \AA}$, which is larger than 10 σ (37.41 \AA).

There are many instances where the volume expansion technique is not practical, notably liquid-liquid equilibria, systems with high vapor pressures (where a significant portion of the liquid will need to evaporate), mixtures with large number of components, etc. An alternative is to design the simulation cell from the onset as a rectangular parallelepiped with $L_x \times L_y \times (3 \text{ to } 10)L_x$. In order to define the L_x dimension, an average *global* density of the fluid is used. As an example, for the case of liquid-vapor system, the initial density average is $\rho = (\rho^V + \rho^L)/2$. Using this value of density and the number of molecules, M , it is possible to calculate the total volume, V ($V = M/\rho$) and $L_x = (V/(3 \text{ to } 10))^{1/3}$. This initial configuration is simulated at high temperature (above the critical state) to homogenize the system. After a few steps (e.g., 50 000 steps), the temperature of the simulation is abruptly scaled to the final temperature (hence the name of temperature quench

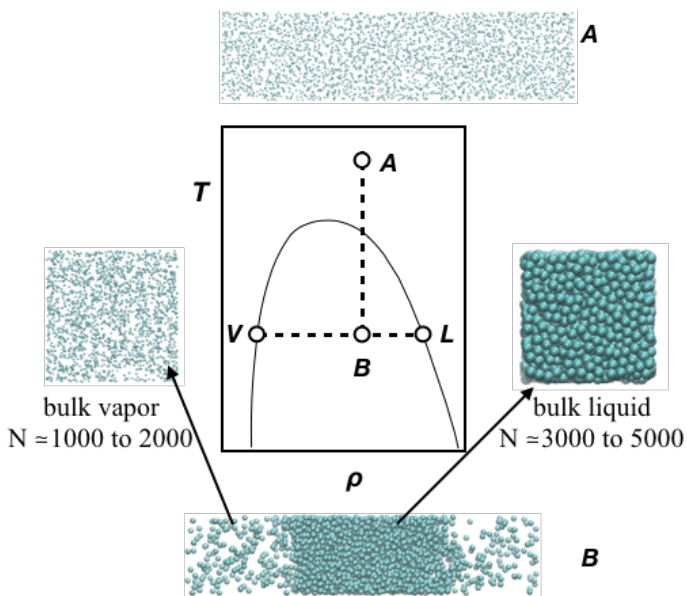


Figure 6. Preparation of the initial box. In the temperature quench strategy, one starts with a system with overall initial density and temperature such that the system is in a one phase mixed state (point A). Upon a rapid decrease in temperature, the system becomes trapped in a metastable state (B) where it spontaneously separates into two distinct phases (V & L).

[70]). If the initial density is chosen appropriately, the system is left in a state of mechanical instability and separates into coexisting equilibrium phases, equilibrating by diffusion, as shown in Fig. 6.

In either case mentioned above, the final outcome is an elongated simulation box with slabs containing the two coexisting phases. A point to consider is the use of an appropriate number of particles to describe not only the liquid and vapor (or second liquid) bulk phases but also the interfacial region. The resulting density profiles should show significant flat density regions for each bulk phase and sufficient molecules in the sparse (vapor) phases to provide for adequate statistics. Sec. 7.1 discusses some typical pitfalls.

For the case of pure fluids in vapor – liquid equilibria, it is not necessary to specify the values of N^L and N^V , it is only necessary to define $N^T = N^L + N^V$, as the system naturally evolves to the liquid-vapor distribution. For the case of fluid mixtures in vapor – liquid equilibria, it is necessary to take into account the total number of particles for each component in all phases (*i.e.*, $N_i^T = N_i^L + N_i^V$). In order to calculate N_i^T , it is advised to consider not only the total number of particles in each phase (N^L and N^V) but also their composition. The compositions in N^L and N^V are given by the corresponding mole fractions in the liquid (x_i) and vapor (y_i) state. The same idea can be applied for the case of mixtures in liquid-liquid equilibria.

EXAMPLE 2: Selection of simulation box size and number of particles for a mixture

Let us to consider a CO_2 (1) + $n\text{-C}_{10}\text{H}_{22}$ (2) mixture at 344.15 K and 3.47 MPa. The available information [71] suggests that at these conditions, the expected mole fraction in the liquid and vapor phases are $x_1 = 0.262$ and $y_1 = 0.994$, respectively, and the mass densities of the phases are $\rho^V = 62.9 \text{ kg/m}^3$ and $\rho^L = 698.7 \text{ kg / m}^3$. Considering the mole fractions and the molecular weight for the pure fluids ($M_w\text{CO}_2 = 44.01 \text{ kg/kgmol}$, $M_w\text{n-C}_{10}\text{H}_{22} = 142.282 \text{ kg/kgmol}$), the average molecular weight of the mixture in the liquid and vapor phase are $M_w\text{liquid} = 116.535 \text{ kg/kgmol}$ and $M_w\text{vapor} = 44.6 \text{ kg/kgmol}$, respectively. Therefore, the molar densities of the mixture are $\rho^V = 1.410 \text{ mol/L}$ and $\rho^L = 5.996 \text{ mol/L}$, hence $(\rho^V + \rho^L)/2 = 3.703 \text{ mol/L}$.

Fluids can be described with coarse grained potentials, where CO_2 is modelled as a single sphere $\sigma_1 = 3.741 \text{ \AA}$ [8, 69] and n -decane as a chain of three spheres, each with a size (diameter) constant of $\sigma_2 = 4.629 \text{ \AA}$ [8].

In this example, initially, $N_t^L = N_1^L + N_2^L = 4150$ particles (beads) in the liquid phase and $N_t^V = N_1^V + N_2^V = 1850$ particles in the vapor phase. While these numbers are in principle arbitrary, as a starting point one can consider around 2000 to 5000 particles for the liquid (N^L), whereas for the vapor phase 1000 to 2000 particles (N^V) could suffice. Smaller systems tend to promote oscillations in the vapor pressure and interfacial tension results [66–68]; larger systems will be computationally more expensive.

The number of molecules of each species N_i is calculated by employing the mole fraction definition and the mass balance expressions and rewriting them it in terms of particles and the number of sites of each component. The final expression for N_1^L is given by:

$$N_1^L = \frac{x_1 N_t^L / f_2}{\frac{1}{f_1} - \frac{x_1}{f_1} + \frac{x_1}{f_2}} \quad (14)$$

where f_i denotes the number of particles that conform the component i . In this example, $f_1 = 1$, $f_2 = 3$, therefore:

$$N_1^L = \frac{0.262 \times 4150 / 3}{\frac{1}{1} - \frac{0.262}{1} + \frac{0.262}{3}} \approx 439 \quad (15)$$

Considering the value of N_t^L , $N_2^L = 4150 - 439 \approx 3711$ particles or $N_2^L = N_2^V / f_2 \approx 1237$ molecules. For the case of vapor phase, similar procedure can be followed replacing N_1^L by N_1^V and x_1 by y_1 giving $N_t^V = 1850$, $N_1^V \approx 1817$ and $N_2^V \approx 33$. In summary, the box can be built with a total of 2256 CO_2 molecules and 1248 n -decane molecules.

Considering these values, the simulation volume can

be calculated from:

$$\begin{aligned} V &= \frac{(6000 \text{ molecules}) \left(10^{10}\right)^3 \left(\frac{\text{\AA}}{\text{m}}\right)^3}{3.703 \left(\frac{\text{mol}}{\text{L}}\right) (N_{\text{av}}) \left(\frac{\text{molecules}}{\text{mol}}\right) (1000) \left(\frac{\text{L}}{\text{m}^3}\right)} \\ &\approx 2690600 \text{\AA}^3 \end{aligned} \quad (16)$$

In this case, $V = L_x \times L_y \times L_z$, $L_x \approx 76.5 \text{ \AA}$ and $L_z = 459.0 \text{ \AA}$. As in the previous examples, it is important to verify that L_x will be larger than $10 \sigma_{\text{max}}$ (46.29 \AA). This initial simulation box is heated to an arbitrarily high temperature, significantly higher than the critical temperature of the mixture (e.g., 1000 K). A subsequent quench of the mixed system to the final temperature produces a two phase split. This design of simulation cell was used to describe the interfacial behavior in CO₂ + n-decane [8]. In the supplementary material, some examples of initial configurations are included.

For multicomponent systems, the quench methods do not allow the *a priori* specification of the bulk compositions, as these derive from the liquid-vapor equilibria. Even in the case where the equilibrium conditions are known and this information is used to build the initial boxes, the excess adsorption at the interfaces will change the initial compositions. Some trial and error, or very large systems where the interfacial volume is much smaller than the bulk will be needed in such cases. Similarly, in cases where the composition of a given component in the mixture is very small, there is the need to run increasingly larger systems for the coexisting phases to be statistically representative.

From a practical perspective, most of the popular molecular simulation software suites provide auxiliary codes or GUI to build the initial configurations. Additionally, the density for pure fluids and fluid mixtures can be found in specialized journals (*i.e.*, Fluid Phase Equilibria (<https://www.journals.elsevier.com/fluid-phase-equilibria>), Journal of Chemical Thermodynamics (<https://www.journals.elsevier.com/the-journal-of-chemical-thermodynamics>), Journal of Chemical & Engineering Data (<https://pubs.acs.org/journal/jceax>), etc) or databases such as DIADEM-DIPPR (<https://dippr.aiche.org>), NIST [54] (<https://www.nist.gov/mml/acmd/trc/thermodata-engine/srd-nist-tde-103b>), or DECHEMA (<https://i-systems.dechema.de/detherm/>). Alternatively, the density can be estimated using a reference equation of state (*e.g.* GERG-2008 [72]), or a molecular-based equation of state, such as SAFT [73, 74]. Versions of the latter model have been implemented in process simulation software such as Aspen (<https://www.aspentechnology.com/en/products/engineering/aspen-plus>) or gProms (<https://www.psenterprise.com/products/gproms>).

5 Simulation details

5.1 Selection of Ensemble

Perhaps the most common ensemble to obtain interfacial properties for a pure component is the canonical (*NVT*) ensemble, where the number of molecules N , the volume V and the temperature T are kept constant. For a mixture, the added degrees of freedom suggest that apart from keeping the compositions and the temperature, an added constraint is needed, namely the pressure P . While an isobaric-isothermal (*NPT*) ensemble would seemingly be appropriate, this ensemble is based on isometric changes in the volume of the box. In the case of systems with interfaces, this would amount to changing the interfacial area, which brings in additional stresses due to the effects of the interfacial tension. Furthermore, the pressure in these heterogeneous systems is not a scalar, but rather a tensor, with different values for the elements of the tensor associated to the different Cartesian directions. For mixtures the *NP_{zz}AT* ensemble is the recommended choice. In this ensemble, the normal pressure (which is the component of the pressure tensor in the direction perpendicular to the interface and corresponds to the bulk pressure) is maintained constant by modifying the L_z dimension of the box keeping the interfacial area, A , constant (equivalently keeping L_x and L_y fixed). We note in passing that application of the Gibbs phase rule suggests that the *NP_{zz}AT* ensemble can only be employed for mixtures, not for pure components. Other alternative ensembles are available [34] whereby the tangential pressure and/or the tension is kept fixed, but are seldomly used.

5.2 Thermostat and Barostat

For any ensemble employed (barring the microcanonical) it is necessary to use a *thermostat* to fix the temperature and/or a *barostat* to fix the pressure. In general terms, these constrains (T, P) are obtained modifying the Hamiltonian expressions of movement by adding an artificial coupling. The commonly used thermo/barostats are those proposed by Nosé and later modified by Hoover, the Nosé-Hoover [75], however there is a trend to employ more advanced propositions such as those by Martyna-Tobias-Klein [76] who use a series of Nosé-Hoover thermostats to construct a Nosé-Hoover "chain". The choice of coupling is critical to the outcome of the simulation [77] and an inappropriate use can give rise to results which are biased or even unphysical [78], *e.g.* the use of the Berendsen thermostat [79], once popular, is now generally discouraged [80] as it does not guarantee the bulk phases to be in equilibrium, thus providing incorrect boundary conditions for the interface.

The strength or magnitude of the coupling is expressed in terms of the thermostat or barostat constant, τ , which is usually given in time units. In order to define the appropriate

value of the thermostat or barostat constant, one can run several MS with different values of τ aiming at ensuring that the total, kinetic, and potential energy reach a stationary value (τ_{\min}). Therefore, $\tau > \tau_{\min}$ assures a stable simulation, while smaller values provide for unphysical fluctuations. Unsurprisingly, the value of the thermostat/barostat constant is an extensive quantity and a function of the particular system and the best advice is to select this value by using this simple test. As a guideline reference one may use values of τ of 0.5 to 2 ps (Nosé-Hoover) for the case of the thermostat, and 0.2 to 1 ps (Nosé-Hoover) for the case of the barostat. Note however that for certain combinations, such as Nosé-Hoover with Parrinello-Rahman, it may be necessary to have $\tau_p > 1.5\tau_t$ to avoid unphysical interactions between the thermostat and barostat. There are no particular special considerations to be taken into account in terms of the thermo/barostats for interfacial systems, hence general suggestions applicable to bulk MS uphold. For an excellent discussion concerning thermostats and barostats, the reader is referred to the textbook by Tuckerman [81].

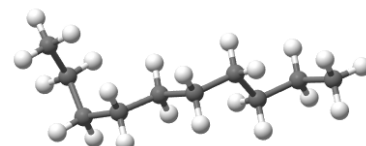
5.3 Force Fields

In MS, the force field follows from the description of the molecule and defines its interactions with other molecules. In general terms, the potential energy U is given by the sum of intramolecular and intermolecular contributions, where the potential is a function of the distance r between individual pairs of molecule segments, the angle θ spanned between triplets of segments, as well as the electrostatics. To wit, the general form of the potential can be written as [15, 82]:

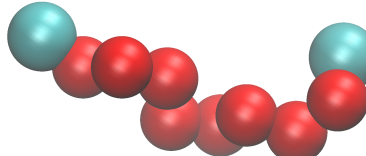
$$U = U^{str}(r) + U^{bend}(\theta) + U^{torsion}(\theta) + U^{vdW}(r) + U^{el}(q, \mu) + U^{pol}(\mu, \alpha) \quad (17)$$

where the intramolecular contributions are the stretch (U^{str}), the bending (U^{bend}), and the torsional ($U^{torsion}$) potentials whereas the intermolecular contributions are the van der Waals or attraction-repulsion (U^{vdW}), the electrostatic (U^{el}), and the polarization (U^{pol}) potentials, among others.

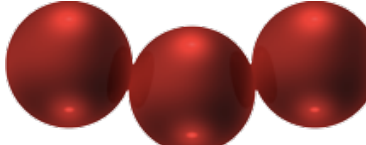
The stretch contribution is usually described by a rigid bond between two consecutive atoms or by a spatial harmonic function, other descriptions including an exponent decay (e.g. the Morse potential). The bending contribution is given by an angular harmonic function. The torsional contribution is expressed as two or three terms of a Fourier series. The van der Waals contribution is built by the two terms attraction and repulsion between atoms in inverse powers forms (e.g. Lennard-Jones and Mie potential) and/or exponential forms (e.g. Buckingham or Hill potential). The electrostatic contribution is usually described by the point charges (e.g. Coulomb potential) and point multipoles. The polarization contribution contains dipole moment, charges, or multipoles.



(a) All Atoms (AA)



(b) United Atoms (UA)



(c) Coarse-grained atoms (CG)

Figure 7. Plausible molecular descriptions for n-C₁₀H₂₂

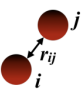
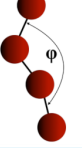
As the previous paragraph illustrates, is often the case that the potential is a smooth function, but this is not a requirement. E.g. the square-well potential is a classic example where U is discontinuous. In such cases special care must be taken in evaluating the interfacial properties, see e.g. [83].

In classical atomistic simulations, there are broadly speaking three different levels of detail used to describe a molecule: all atoms (AA), whereas the name implies, all individual atoms are represented by centers of force; united atoms (UA), where the hydrogen atoms are included in the representation of the associated heavier atoms and coarse-grained (CG) representations, where larger groups of atoms, typically incorporating three to four heavy atoms and their associated hydrogens are represented in a single bead. Fig. 7 displays models for n-decane (n-C₁₀H₂₂) for all three strategies.

One can see from Fig. 7 that it is necessary to track a total 32 particles (and possibly an equal number of partial charges) in an AA description; 10 particles in the UA description and only 3 in a CG description of n-C₁₀H₂₂. Considering that the interaction between two single molecules at close range involves the calculation of the square of these interactions, it is evident how rapidly the use of UA and CG models imply orders of magnitude speedup in the MS, as more than 90% of the time in a MS code is spent in the evaluation of the force fields. The crux of the matter is not to lose accuracy for the sake of computational efficiency. The selection of the level of description depends on the properties of interest, but thankfully for the case of interfacial properties, UA and even CG seem more than adequate⁵. In many cases for simple

⁵See for example the results of the 9th Industrial Fluid Properties Simulation

Table 2. Contribution to the potential energy in the TraPPE UA for n-C₁₀H₂₂. k_B is Boltzmann's constant. θ is the bond angle between three consecutive united-atoms, and subscript 0 denotes its equilibrium value. ϕ is the dihedral angle between four consecutive united-atoms. r_{ij} is the distance between united-atoms i and j. ϵ_{ij} is the energy parameter of the interaction, whereas σ_{ij} is the Lennard-Jones size parameter.

description	equation	values
	$U^U(r) = 4\epsilon_{ij} \left[\left(\frac{\sigma_{ij}}{r_{ij}} \right)^{12} - \left(\frac{\sigma_{ij}}{r_{ij}} \right)^6 \right]$ $\epsilon_{ij} = \sqrt{\epsilon_{ii} \epsilon_{jj}}$ $\sigma_{ij} = (\sigma_{ii} + \sigma_{jj}) / 2$	$\epsilon_{CH3} / k_B = 98 \text{ K}$ $\epsilon_{CH2} / k_B = 46 \text{ K}$ $\sigma_{CH3} = 3.75 \text{ \AA}$ $\sigma_{CH2} = 3.95 \text{ \AA}$
	$U^{bend}(\theta) = \frac{k_\theta}{2} (\theta - \theta_0)^2$ $\theta_0 = 114.0^\circ$	$k_\theta / k_B = 62500 \text{ K/rad}^2$
	$U^{torsion}(\varphi) = c_1 (1 + \cos \varphi) + c_2 (1 - \cos 2\varphi) + c_3 (1 + \cos 3\varphi)$	$c_1 / k_B = 355.0 \text{ K}$ $c_2 / k_B = -68.19 \text{ K}$ $c_3 / k_B = 791.3 \text{ K}$

fluids, the reduction in the fidelity of the model does not have an influence on the accuracy of the results. Some detail is obviously lost upon coarse-graining, which might be relevant if the onus is on exploring the interfacial orientation and /or charged fluids. In these cases, the use of UA models seems an acceptable compromise.

EXAMPLE 3: Selection of force field

The molecule description, its values, and restrictions depend on the type of force field used. As an example, the UA force field for n-C₁₀H₂₂ can be described by using the TraPPE-UA model (<http://chem-siepmann.oit.umn.edu/siepmann/trappe/index.html>). In this case, the potential energy is described by Eq. 17 reduces to

$$U = U^{str}(r) + U^{bend}(\theta) + U^{torsion}(\varphi) + U^U(r) \quad (18)$$

In TraPPE-UA, the stretch contribution is described by a rigid bond between two consecutive united-atoms with a length of 1.54 Å for the case of decane. The remaining terms are summarized in Table 2. Here k_B is Boltzmann's constant. θ is the bond angle between three consecutive united-atoms, and subscript 0 denotes its equilibrium value. φ is the dihedral angle between four consecutive united-atoms. r_{ij} is the distance between united-atoms

Challenge (<http://fluidproperties.org>) where a blind test of the capabilities of diverse force fields was performed by predicting the interfacial tension of oil/water systems at high temperatures and pressures. Coarse Grained models [21] fared as well as more detailed UA and AA models [22, 23]. See also Ref. [69] for an example relevant to this manuscript.

i and j. ϵ_{ij} is the energy parameter of the interaction, whereas σ_{ij} is the Lennard-Jones size parameter.

In the case of a CG force field, n-C₁₀H₂₂ can be represented by three tangential spheres. Using the Mie potential (See Ref. [84] and references therein), these spheres interact with each other according to:

$$U(r) = C \epsilon_{ij} \left[\left(\frac{\sigma_{ij}}{r_{ij}} \right)^{\lambda_{r_{ij}}} - \left(\frac{\sigma_{ij}}{r_{ij}} \right)^{\lambda_{a_{ij}}} \right] \quad (19)$$

$$C = \left[\frac{\lambda_{r_{ij}}}{\lambda_{r_{ij}} - \lambda_{a_{ij}}} \left(\frac{\lambda_{r_{ij}}}{\lambda_{a_{ij}}} \right)^{\frac{\lambda_{a_{ij}}}{\lambda_{r_{ij}} - \lambda_{a_{ij}}}} \right]$$

where $\lambda_{r_{ij}}$ and $\lambda_{a_{ij}}$ are the repulsion and attraction parameters of the intermolecular potential, respectively. r_{ij} is the center-to-center distance of the interacting segments. ϵ_{ij} is the energy scale corresponding to the potential well depth, σ_{ij} is the length scale, corresponding loosely with an effective segment diameter. The Mie potential reverts to the well-known Lennard-Jones model if the repulsive and attractive exponents are taken as 12 and 6, respectively. For the case of n-C₁₀H₂₂ the Mie parameters are [8]: $\lambda_{r_{ij}} = 19.21$, $\lambda_{a_{ij}} = 6$, $\epsilon_{ij} / k_B = 414.90 \text{ K}$ and $\sigma_{ij} = 4.629 \text{ \AA}$.

For the case of heteronuclear molecules or mixtures, the cross parameters for the Mie are obtained by using the following combination rules:

$$\sigma_{ij} = (\sigma_{ii} + \sigma_{jj}) / 2 \quad (20)$$

$$\epsilon_{ij} = (1 - k_{ij}) \frac{\sqrt{\sigma_{ii}^3 \sigma_{jj}^3}}{\sigma_{ij}^3} \sqrt{\epsilon_{ii} \epsilon_{jj}} \quad (21)$$

$$(\lambda_{k_{ij}} - 3) = \sqrt{(\lambda_{k_{ii}} - 3)(\lambda_{k_{jj}} - 3)} \quad (22)$$

where $\lambda_{k_{ii}} = \lambda_{r_{ii}}$ or $\lambda_{a_{ii}}$, etc., and k_{ij} is a binary interaction parameter, which can be obtained from experimental data of phase equilibria.

In the supplementary information, the force field for the CO₂ and n-C₁₀H₂₂ pure fluids as well as for the CO₂ + n-C₁₀H₂₂ mixture are included for both TraPPE-UA and CG-Mie schemes.

5.4 Cutoff radius and long range corrections

The most time-consuming aspect of any simulation is related to the calculation of the nonbonded (van der Waals or long-range interactions) terms in the potential energy function. Approximately, the number of interactions that must be calculated scale with the square of the number of force centers (although with the use of elaborate algorithms this may be scaled down). In order to reduce the calculation time associated with the evaluation of these long-range interactions,

a truncation of the energy (or force) is used. In other words, the energy (or force) is set to zero for distances larger than a given radius, traditionally called the cutoff radius (r_c). One option is to cut the potential at r_c . Another option is switching the tail off smoothly, which makes the potential energy zero after a given r_c .

Ideally, one would not need to consider a cutoff radius and would calculate the interaction between all particles in the simulations cell. Many of these interactions correspond to pairs of molecules which are at a significant distance from each other and essentially do not interact. Fig. 8 shows the effect of a cutoff radius, where the calculation of forces is only taken into account for molecules whose centers are at a distance $r < r_c$ apart. Note however that the application of a cutoff is, in effect, modifying the potential (and consequently the results) hence the balance between the speed up of the calculation and the accuracy of the results is important. Excellent discussions of this topic have been provided in Ref. [32, 39, 40, 42, 85]

In homogeneous systems, the application of short cutoffs can be offset by adding long range corrections (LRC) based on a mean field value. For the case of inhomogeneous systems, clearly this must be done with attention, particularly for molecules in the vicinity of interfacial region where different environments are present at either side of the interface [86–89]

For most simple systems, given the current availability of cheap computer power, a suitable practice for MS of interfacial properties is to use large cutoffs rather than to have to correct the results. In the case of massive systems or to reduce computational demand, shorter cutoffs with inhomogeneous large range correction could be included with care. For specific details concerning to this implementation, the reader is redirected to the elegant work of Martínez-Ruiz et al. [90] for the case of MD and Ibergay et al. [91] for the case of MC.

In order to define the value of the cutoff, it is advised to run a few simulations to define the lower value to capture the interfacial properties. As an example, Fig. 8 typifies the impact of cutoff in bulk and interfacial properties.

From this figure, it is seen how at larger r_c all properties of relevance reach a stationary value. Clearly, the large cutoff can never be more than half of the smallest cell dimension (e.g., $L_x/2$). Therefore, as a suggestion, a value of cutoff equal or larger than $6\sigma_{\max}$ (typically ≈ 2 nm) will be an adequate choice to avoid the truncation and system size effects involved in the phase equilibrium and interfacial properties calculations.

For the case of fluids with electrostatic contributions to the energy, the potential energy decays proportional to r^{-1} (rather than r^{-6} as in the case of simple dispersion). In this

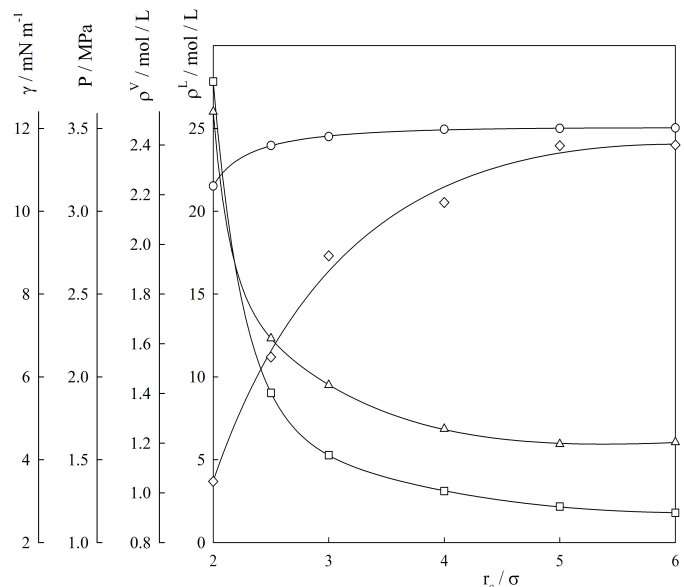


Figure 8. Impact of cutoff (r_c) on the bulk and interfacial properties for the case of CO₂ (single Mie sphere, $\epsilon/k_B = 353.55\text{K}$; $\sigma = 3.741\text{\AA}$; $\lambda_r = 23.0$; $\lambda_a = 6.66$) at 240 K. ◇, surface tension γ ; △, vapor pressure P ; ○, liquid density ρ^L ; □, vapor density ρ^V .

case, the definition of "a short distance r_c where the potential tails to effectively a zero value", ceases to make sense.

The naïve solution suggests using a simulation cell with very long dimension L_x ($r_{c,max} = L_x/2$). Unfortunately, such large L_x implicates a very (very) big simulation box, both impractical and ultimately unnecessary. This issue can be solved by using a numerical strategy that converts the real space to the reciprocal (or complex) space effectively providing for an alternative force calculation. The most popular of said methods, Ewald summation [92], proposes to neutralize each partial charge in the fluid by a superposition of spherical Gaussian distributions of opposite charge while employing a second Gaussian of similar charge to the original to annul the effect of the first set. The resulting potential stemming from these Gaussians is obtained from Poisson's equation and is solved as a Fourier series. This combination provides a route to replace the real space (where r_c would be very large) to a combination of real, and reciprocal (or complex) space. In practice, Ewald's methodology is controlled by three variables: the real space cutoff (r_c); the convergence parameter and the largest reciprocal space vector used in the reciprocal space sum. The convergence parameter and reciprocal space vector are obtained using a minimization procedure, which uses the Coulombic energy and the Coulombic virial. From a technical view point, a very efficient algorithm for optimization is implemented in DL_POLY software, where these parameters are obtained when the simulation starts. Ewald summations are time consuming from a point of view of the MS so efforts to re-

duce the simulation time are in continuous development (e.g. reaction field [93, 94], the smoothed particle mesh [95], and the Wolf [96] methods; see further details in Ref. [15]). While the electrostatic potentials are the prototypical examples of long-ranged potentials, some very soft potentials (e.g., an 8-6 Mie) will also exhibit relatively long attractive tails, for which Ewald summations can also be applied in order to avoid the use of calculating long range corrections [97].

5.5 Simulation length

Simulations are divided into two stages: equilibration and production. During the equilibration, the thermostat and/or barostat force the system to reach the desired thermodynamic state conditions. In the subsequent production stage, the thermostat and/or barostat are commonly (although not necessarily) turned off, and the system naturally evolves in *NVE* ensemble, where statistics are collected. It is advised that the production length is at least twice the equilibration stage.

In the case of MS based on MD, the simulation length is usually defined in terms of the requested time or the total number of steps using a defined time step. The specification of the time step is a function of the stability of the numerical algorithm used to integrate the Newtonian equations.

Small values of the Δt are not efficient because the dynamics take too long time to achieve the simulation time, whereas larger Δt produces unstable dynamics due to the high errors involved in the integration. Therefore, the selection of the appropriate Δt for the particular system needs to be defined. Fincham [98] proposed an empirical but useful method to define the optimal value of the Δt . The main idea of this method is to run a series of simulations from the same equilibrated state, but each one with different Δt . For each simulation, the potential energy is evaluated with its standard error. The selected Δt is the largest one with low standard error. Another option to define Δt has been proposed by Kim [99] who proposed to use a size of about 0.0333 to 0.01 of the smallest vibrational period in the simulation.

Considering these guidelines, as well as the existing body of literature on MD for interfacial properties, one observes that the Verlet leapfrog algorithm is commonly used with a time step from 0.003 to 0.01 ps. As another point of reference, an order of magnitude estimate of the time step can be had from the following equation for Lennard-Jones fluids:

$$\Delta t = 0.01 \sqrt{\frac{m \sigma^2}{\varepsilon}} \quad (23)$$

where m , ε , and σ take their usual meaning (as in the LJ potential). For the particular case of interfacial properties of pure fluids, simulations are typically longer than those of one phase bulk fluids, namely because of the requirement of the establishment of the interface and the relatively slow diffusion of components through the otherwise large systems. For

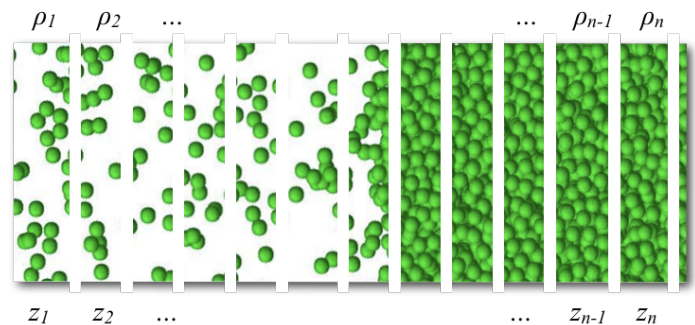


Figure 9. Partitioning of the simulation box in n vertical slabs for computing the density profile, ρ_i .

pure components, 10 to 15 ns for the equilibration stage, and 30 ns for the production state are common times. For the case of mixtures, a longer equilibrations are needed, to the tune of 70 to 80 ns after which production runs should be set for at least another 150 ns.

In the case of MC simulations, the simulation length is usually defined in terms of the number of cycles, where each cycle consists of N randomly selected moves that include translation, rotation, flips, etc. A typical MC run in the *NVT* or $NP_{zz}AT$ ensemble consists of $O(10^6)$ cycles for equilibration and $O(10^7)$ cycles for production.

6 Post-processing

Interfacial tensions and associated properties are rarely calculated on-the-fly, but rather obtained from post-processing the results of a MS. This section is devoted to describing the calculation of the interfacial density, concentration profiles and the interfacial tension. Additionally, the evaluation of other derived properties, such as isothermal Gibbs adsorption and surface entropy and surface enthalpy are illustrated.

6.1 Calculation of interfacial density profiles and related interfacial properties

The density profile is calculated by dividing the simulation box ($L_x L_y L_z$) in n slabs ($n \approx 250$ to 500) along the z direction, as it is illustrated in Fig. 9. At each position, the density of a molecule i in the slab j , ρ_{ij} is calculated as:

$$\rho_{ij} = \frac{\langle N_i \rangle}{V_j} = \frac{(\sum_{s=1}^{ns} N_{is}) / ns}{V_j} \quad (24)$$

where N_i is the number of molecules i in the j slab; s represents the sites of the molecule i , and ns is the number of sites per molecule. V_j is the volume of each slab, which is $L_x L_y L_{zj}$. As an example, the density of $n\text{-C}_{10}\text{H}_{22}$ in the slab j can be calculated as $\rho_j^{\text{C10H22}} = ((N_j^{\text{CH3}} + N_j^{\text{CH2}})/10)/V_j$ for the case of UA whereas $\rho_j^{\text{C10H22}} = (N_j/3)/V_j$ for the case of CG model. Note that we suggest to calculate the densities based on the number of

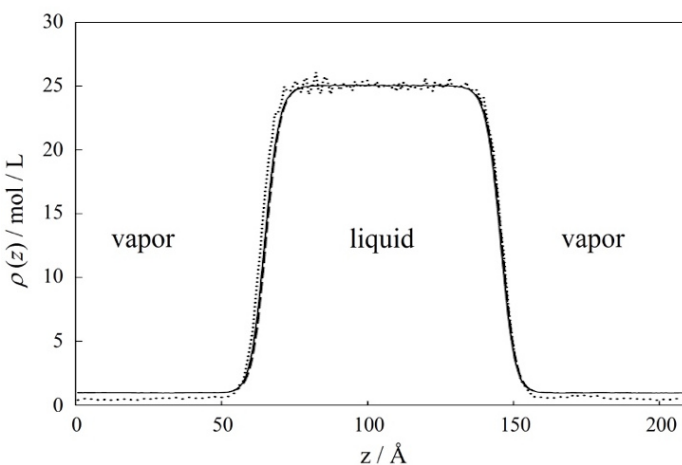


Figure 10. Time evolution of ρ vs z profiles for the case of CO_2 (single Mie sphere, $\epsilon/k_B = 353.55\text{K}$; $\sigma = 3.741\text{\AA}$; $\lambda_r = 23.0$; $\lambda_a = 6.66$) at 240 K at vapor – liquid equilibria. (•••) 18 ns, (--) 36 ns, and (—) 54 ns.

sites observed in a given slab. In most cases of chain fluids, molecules will span several slabs, and this must be accounted for.

In order to guarantee that the simulated systems are at a true equilibrium state, neither transient nor steady state, it is advised to monitor the time evolution of the concentration of species in the direction normal to the interface, $\rho_i(z)$. Holcomb *et al.* [32] demonstrated that the time evaluation of $\rho_i(z)$ can bring not only a picture of the progression to equilibrium but also provides a way to establish a true equilibrium condition. Fig. 10 shows the time evolution of $z - \rho_i(z)$ for the case of CO_2 represented as single Mie sphere (see Ref. [10] for the case of Lennard – Jones fluid.)

From this figure, we can observe that as the simulation time increases, the density in the bulk regions plateau while the interfacial regions adjust their shape until eventually reaching a steady state (after 36 ns in the example in Fig. 10).

It is possible that systematic round-off errors in the simulation induce a drift in the position of the slabs. If this is not corrected or accounted for, the density profiles might be smeared out and interfacial widths misrepresented. A trick of the trade is to re-center the center of mass of the system every once in a while, or to periodically zero out the total momentum of the system, to avoid these spurious effects.

The interfacial profiles for pure fluids and also for fluid in mixtures without surface activity can be fitted using Eq. 3 which can also be used directly to provide an estimate of the interfacial thickness. For the case of mixtures, the interfacial concentration of species, $z - \rho_i(z)$ provide a route to evaluate the surface activity of the fluids in mixture. As an illustration, Fig. 11 displays the $z - \rho_i$ projections for the case of $\text{CO}_2 + n\text{-C}_{10}\text{H}_{22}$ mixture at 344.15 K. In this figure, we only include one vapor-liquid interface, as the system is symmetrical along

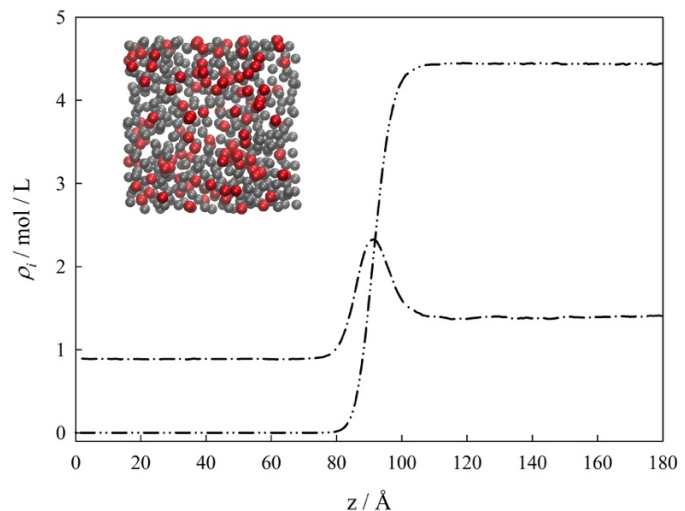


Figure 11. Interfacial profiles for $\text{CO}_2 + n\text{-C}_{10}\text{H}_{22}$ mixture at 344.15 K and $P = 2.39$ MPa ($x_1 = 0.238$). MD results for $--$, $z - \rho_1$; $-.-$, $z - \rho_2$. Insert is a snapshot of the interfacial region, seen from the CO_2 -rich side, depicting only the first layer of adsorbed molecules. CO_2 (red), $n\text{-C}_{10}\text{H}_{22}$ (gray). (adapted from Ref. [8])

the z coordinate (see Fig. 10).

The interfacial profiles provide a method to evaluate the surface activity of the fluids inside the interfacial zone. In the example of Fig. 11, a positive surface activity is seen for CO_2 ($d\rho_1/dz = 0$; $d^2\rho_1/dz^2 < 0$ in the interfacial region), whereas $n\text{-C}_{10}\text{H}_{22}$ does not show surface activity. Additionally, the interfacial density profiles provide the needed information to describe the observed surface activity behavior in terms of the relative Gibbs adsorption isotherm of CO_2 (1) with respect to $n\text{-C}_{10}\text{H}_{22}$ (2), Γ_{12} (see Eq. 4). Again, as an example, for the system and condition of the figure, $\Gamma_{12} = 1.523 \times 10^{-9}$ kmol/m²[8].

6.2 The mechanical route for the interfacial tension: The pressure tensor method

The pressure tensor method is the most common way of calculating the interfacial tension for pure fluids and fluid mixtures. The basis of this method is to calculate the components of the diagonal element of the inhomogeneous pressure tensor, ($P_{xx}(z)$, $P_{yy}(z)$, $P_{zz}(z)$) by using the Irving-Kirkwood (IK) [100] (or alternatively the Harasima [101])⁶ formulation which then feeds into Eq. 1 to be employed to calculate the tension.

In the IK method, the pressure tensor element, $P_{kk}(z)$ is given by the following expression:

$$P_{kk}(z) = k_B T \rho(z) + \frac{1}{A} \left\langle \sum_{i=1}^{N-1} \sum_{j>i}^N \frac{1}{|z_i - z_j|} (f_{ij}(z))_k (r_{ij})_k \right\rangle \quad (25)$$

⁶For a concise discussion on the strategies of calculating the pressure tensor, including the IK and Harasima definitions, the reader is referred to Ref. [102].

In Eq. 25, the subscript kk represents the spatial coordinate, either x , y , or z , k_B is Boltzmann's constant, T is the absolute temperature, A is the interfacial area, N is the number of molecules, and the double sum involves the force on molecule i due to molecule j . f_{ij} is the force on molecule i due to molecule j , and r_{ij} represents the distance between molecules i and j . It is important to note that Eq. 25 sums two terms. The first term takes into account the kinetic contribution, which is proportional to the ideal-gas pressure, while the second term corresponds to the configurational contribution which is evaluated as *ensemble averages*, as indicated by the $\langle \dots \rangle$ brackets, and not instantaneous values.

In MD codes, the most common implementation of the algorithm is to evaluate the average of the elements $\langle P_{kk} \rangle$ over the *whole volume* of the simulation box. Speculating over the possible reason for this implementation of $\langle P_{kk} \rangle$ is the inspiration on the pressure calculation in homogeneous systems, where the pressure of the system is given by the arithmetic average of the diagonal elements: $P = (\langle P_{xx} \rangle + \langle P_{yy} \rangle + \langle P_{zz} \rangle)/3$, (*i.e.* the trace divided by 3). As an illustration of the underlying issue, Fig. 12 displays the diagonal elements of the pressure tensor $\langle P_{xx} \rangle$, $\langle P_{yy} \rangle$, and $\langle P_{zz} \rangle$ evaluated for the whole volume of a simulation box in an inhomogeneous system during the production stage, where it is possible to observe that this implementation produces artificial fluctuations in the results. The values of $\langle P_{xx} \rangle$ and $\langle P_{yy} \rangle$ vary only along the z coordinate, whereas $\langle P_{zz} \rangle$ should be constant along z , implying that the normal pressure (that of the bulk phases) is $P_N = \langle P_{zz} \rangle$ while the tangential components will be equal (due to the symmetry of the problem) $P_T = \langle P_{xx} \rangle = \langle P_{yy} \rangle$.

Considering the values reported in Fig. 12 and averaging their values over the production stage, one obtains $\langle P_{xx} \rangle = 0.4072$ MPa, $\langle P_{yy} \rangle = 0.4043$ MPa, and $\langle P_{zz} \rangle = 1.4691$ MPa. Taking the average of $\langle P_{xx} \rangle$ and $\langle P_{yy} \rangle$ as $P_T = (\langle P_{xx} \rangle + \langle P_{yy} \rangle)/2$, and $P_N = \langle P_{zz} \rangle$, Eq. 1 can be rewritten as:

$$\gamma = \frac{L_z}{2} \left[\langle P_{zz} \rangle - \frac{\langle P_{xx} \rangle + \langle P_{yy} \rangle}{2} \right] \quad (26)$$

In this latter equation the additional factor of $1/2$, takes into account the presence of two interfaces in the system. Evaluating Eq. 26, with $L_z = 208$ Å one obtains $\gamma = 11.059$ mN m $^{-1}$. The values of P_N , and γ are close to the NIST values (*i.e.*, 1.2825 MPa and 11.52 mN m $^{-1}$) [54].

The accuracy of this result is rather surprising and presumably a consequence of the correlation between the fluctuations in the different Cartesian directions. Over the volume of the simulation box, and with the exception of the interfacial region, the difference between the normal and tangential components should be zero (in a statistical sense), hence the unexpected outcome of a correct result upon averaging the curves in Fig. 12.

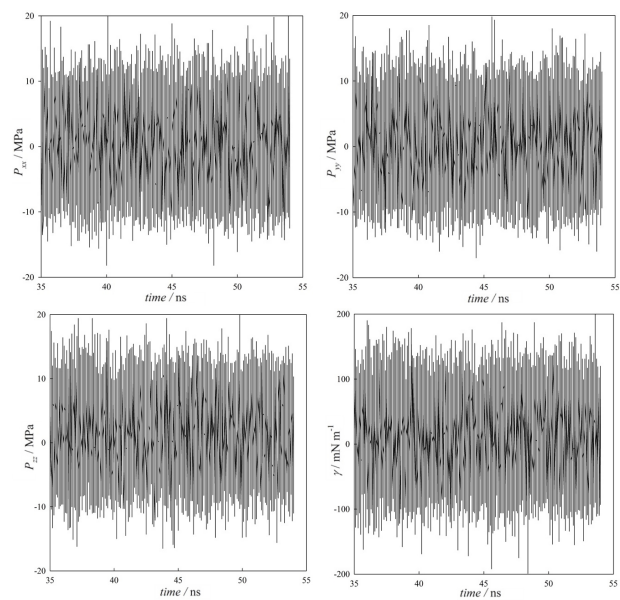


Figure 12. Diagonal elements of the pressure tensor $\langle P_{xx} \rangle$, $\langle P_{yy} \rangle$, and $\langle P_{zz} \rangle$ and the resulting interfacial tension, γ , evaluated over the volume simulation box for the case of CO₂ (single Mie sphere, $\epsilon/k_B = 353.55$ K; $\sigma = 3.741$ Å; $\lambda_r = 23.0$; $\lambda_a = 6.66$) at 240 K. The apparently large fluctuations are typical and showcase some of the issues with the evaluation of Eq. 1.

This method, albeit computationally convenient and accurate, fails to describe the elements of the pressure tensor for medium or strongly inhomogeneous systems and also for inhomogeneous systems with more than two interfaces, such as liquid – liquid – vapor and liquid – liquid – liquid interfaces [10, 24]. Unfortunately, most post-processing tools embedded in the available MD software will rely on this implementation (*c.f.*, Table 1)

An alternative (and preferred) implementation of IK tensor for inhomogeneous systems considers dividing the simulation box ($L_x L_y L_z$) in n slabs ($n \approx 250$ to 500) along the z direction, as it is illustrated in Fig 9 for the case of density. For each slab, the $P_{kk}(z)$ ($kk = xx, yy, zz$) is calculated from Eq. 25, and an ensemble average of each element of the pressure tensor *in each slab* along the z coordinate, $\langle P_{kk}(z) \rangle$ is obtained.

Fig. 13 displays the time evolution of $\Delta\langle P(z) \rangle = (\langle P_N(z) \rangle - \langle P_T(z) \rangle)$ for a typical case of an isothermal VLE. From the pressure elements $\langle P_N(z) \rangle$ and $\langle P_T(z) \rangle$, the interfacial tension, γ , between two bulk phases (*e.g.*, liquid – vapor or liquid – liquid) can be calculated from Eq. 1, which can be rewritten as:

$$\gamma = \int_{-\infty}^{+\infty} \left[\langle P_{zz}(z) \rangle - \frac{\langle P_{xx}(z) \rangle + \langle P_{yy}(z) \rangle}{2} \right] dz \quad (27)$$

Fig. 14 displays the final average of $\gamma = \int \Delta\langle P(z) \rangle dz$ along the interfacial region, z , for vapor – liquid – vapor interfaces. Two plateau regions are evident. The first one corresponds to the first interfacial region (vapor – liquid) and the second

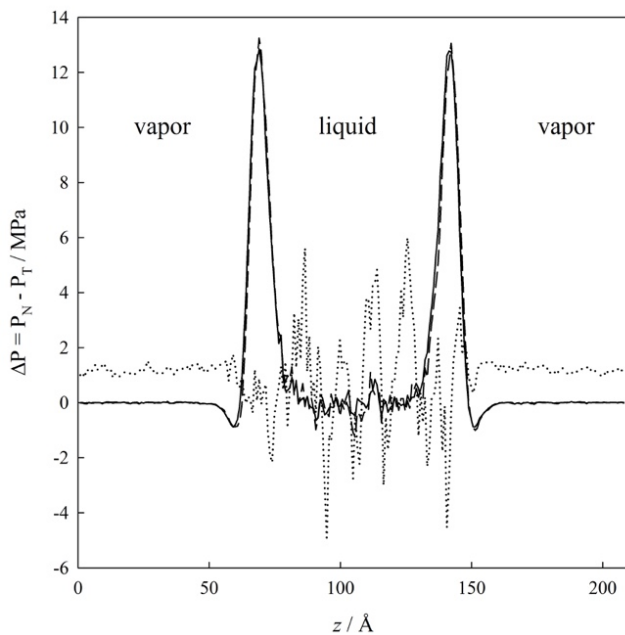


Figure 13. Time evolution of $\Delta P = (P_N - P_T)$ vs z profiles for the case of CO_2 (single Mie sphere, $\epsilon/k_B = 353.55\text{K}$; $\sigma = 3.741\text{\AA}$; $\lambda_r = 23.0$; $\lambda_a = 6.66$) at 240 K at vapor – liquid equilibria. (•••) 18 ns, (--) 36 ns, and (—) 54 ns.

correspond to the second interfacial region (liquid – vapor). The magnitude of the interfacial tension, γ , is directly obtained from this figure, where the first plateau corresponds to γ and the second plateau is the cumulative value of γ (*i.e.*, 2γ). For the case illustrated in Fig. 14, the IK method (Eq. 27) predicts $\gamma = 11.15 \text{ mN m}^{-1}$, which is similar to the value obtained by Eq. 26. The recommended practice for evaluating the magnitude of γ is to use the value of the first plateau rather than the second value. The second value contains all the accumulated error stemming from the liquid phase.

In summary, the evaluation of the magnitude of interfacial tension through the mechanical route (or the pressure tensor) can be carried out by using two types of averages over the diagonal element of the pressure tensor, $P_{xx}(z)$, $P_{yy}(z)$, and $P_{zz}(z)$. The first approach evaluates these elements as an ensemble average of the pressure tensor over the whole volume of the simulation cell, $\langle P_{kk} \rangle$, whereas a second approach calculates them by using an ensemble average of the uppressure tensor along discrete slabs in the z coordinate, $\langle P_{kk}(z) \rangle$. The recommended practice to compute the interfacial tension from the mechanical route is to use the latter method, which not only provides the interfacial tension value but also the normal or equilibrium pressure. Citing Holcomb et al. [32] this route provides information of the time evolution of these variables and can bring not only a picture of the progression to equilibrium, but also provides a way to establish a true equilibrium

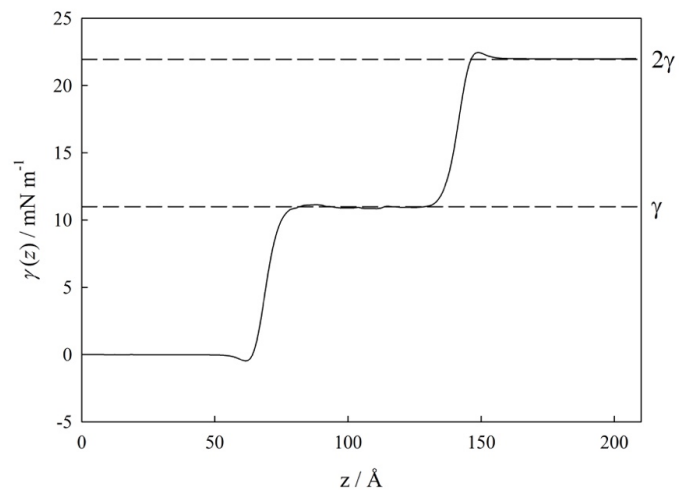


Figure 14. $\gamma = \int \Delta P(z) dz$ along the interfacial region, z , for the case of CO_2 (single Mie sphere, $\epsilon/k_B = 353.55\text{K}$; $\sigma = 3.741\text{\AA}$; $\lambda_r = 23.0$; $\lambda_a = 6.66$) at 240 K at vapor – liquid equilibria.

condition and to evaluate some possible issues related with the initial conditions used (*e.g.*, the positive slope of the first plateau indicates that the initial density was lower than the expected value.)

From a practical viewpoint, the IK tensor has been incorporated in all MD and some MC codes (c.f. Table 1). However, most of them compute $\langle P_{kk} \rangle$, rather than $\langle P_{kk}(z) \rangle$. To the best of our knowledge, only the MD-LAMMPS and the MC-Gibbs codes include both $\langle P_{kk} \rangle$ and $\langle P_{kk}(z) \rangle$ and also compute the interfacial tension according to Eqs. 26 and 27, respectively.

For the other MS codes, it is necessary to include a subroutine able to compute P_{kk} slabs by slabs along the z coordinate. In the supplementary information, DL_POLY and HOOMD subroutines are included for the case of Mie potential.

6.3 Thermodynamic route for the interfacial tension: Test area method

The test area (TA) method provides a perturbative route to calculate the interfacial tension, γ . In order to evaluate Eq. 2, an equilibrated system (state 0) with interfacial area A_0 ($A_0 = 2 L_{x,0} L_{y,0}$) is perturbed by an infinitesimal change in the interfacial area. This perturbation translates the system to a new state (perturbed state or state 1) that has the same volume as the original state, but a different interfacial area. The new interfacial area in state 1 is A_1 , which is obtained using the following transformations $L_{x,1} = L_{x,0}(1 + \xi)^{1/2}$, and $L_{y,1} = L_{y,0}(1 + \xi)^{1/2}$, where $\xi \ll 1$. Using this transformation, $A_1 = A_0 + \Delta A$ and $\Delta A = L_{x,0} L_{y,0} \xi$. In order to guarantee a constant volume condition, L_z needs to change from $L_{z,0}$ to $L_{z,1} = L_{z,0} / (1 + \xi)$. At each state (0 and 1), the configurational energy of the system is calculated, and the difference $\Delta U =$

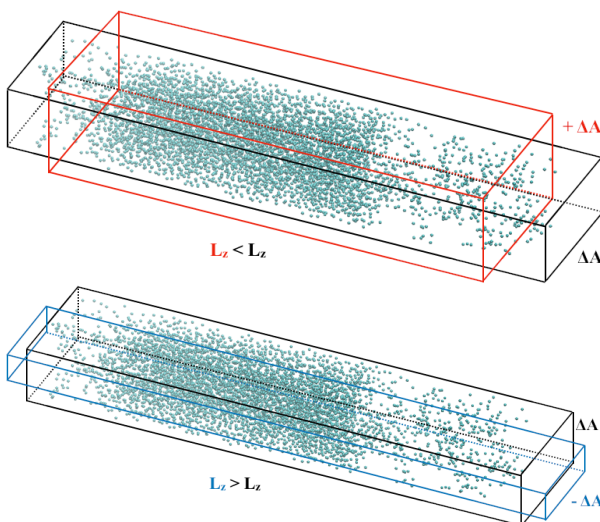


Figure 15. Illustration of the area perturbation. Expanding ($+ \Delta A$) and compressing ($- \Delta A$) the interfacial area.

$U_1 - U_0$ is evaluated. The calculation of γ is carried out by both expanding ($+ \Delta A$) and compressing ($- \Delta A$) the interfacial area, as illustrated in Fig. 15.

The final value of γ for a given $|\Delta A|$ is the result of the average over these two perturbations. A plot of the corresponding Boltzmann average $\langle \exp(-\Delta U/k_B T) \rangle_0$ as a function of the perturbation $|\Delta A|$ allows for the calculation of the limiting value at $\Delta A \rightarrow 0$. The size of the perturbation ξ is key in obtaining meaningful results. Too small a perturbation will inevitably produce changes in energy which are of the order of the machine precision, essentially noise, while too large of a perturbation produces overlaps amongst the molecules and a deviation from the expected linear regime. As a rule of thumb, it is advised to evaluate expansion and compression paths for ξ ranging from 10^{-7} to 10^{-2} . Fig. 16 illustrates the values of γ obtained from MD using the TA for the case of $\text{CO}_2 + n\text{-C}_{10}\text{H}_{22}$ mixture at 344.3 K and $x_1 = 0.448$, where it is possible to observe that γ is constant in the range $10^{-5} < \xi < 10^{-3}$. Using a value of $\xi = 5 \times 10^{-4}$, the $\gamma = 8.46 \text{ mN m}^{-1}$. [9]

Further details concerning to the TA can be found in Ref. [33] for the methodological description, and some application for TA can be found in Ref. [9] for MD simulations and Refs. [26, 31] for MC simulations.

The evaluation of interfacial tension through the thermodynamic route (or the test area method) provides for a calculation of interfacial tension which is distinct and independent of the mechanical route, and can be employed as a test of consistency. Fig. 17 shows the interfacial tension of $\text{CO}_2 + n\text{-C}_{10}\text{H}_{22}$ mixture at 344.3 K as a function of pressure. The MD results have been obtained from IK, and TA methods and their results are favourably compared to experimental data. However, a slight overprediction by the IK and TA methods

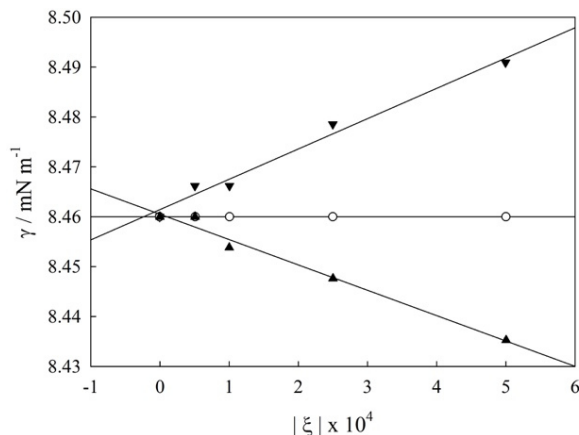


Figure 16. Values of γ for $\text{CO}_2 + n\text{-C}_{10}\text{H}_{22}$ mixture at 344.15 K obtained from MD using the TA method. The results are obtained for different values of the perturbation factor ξ : \blacktriangledown , expansive perturbations, $\xi > 0$; \blacktriangle , compressive perturbations, $\xi < 0$; and \circ , average of the positive and negative perturbations.

can be seen. This systematic deviation could be caused by the combined deviations of pressure and interfacial tension. For further discussion related to these results, the reader should consult Refs. [9, 70].

The TA method has been employed to study phenomena for which the mechanical route is ill suited, such as in the determination of the interfacial tension of discontinuous potentials [33] and drops and bubbles [26, 65]. The TA method will be a poor choice for systems with long chain fluids. Here, the perturbative step is difficult to carry out due to the periodic boundary conditions: operationally, the TA method requires the removal of the periodic boundary conditions, the expansion/compression of the simulation box and finally the recovery of the boundary periodic conditions, steps which can be cumbersome for long chains. Similarly, the method is only valid when one type of interface is present in the simulation box, hence is unsuitable to study three-phase systems.

6.4 Other properties obtained from the interfacial tension

By differentiation of the temperature dependence of the interfacial tension, one can access both the surface entropy (s^γ) and surface enthalpy (h^γ) change of surface formation, Eqs. 9 and 11. This evaluation is carried out by a simple numerical derivation of the MS results. As an example, Fig. 18 illustrates s^γ and h^γ change as a function of temperature for selected n-alkanes.

Additionally, the interfacial tension as a function of temperature can be also used to estimate the critical temperature for pure fluids. In this case, the interfacial tension is correlated with the critical temperature by using the scaling laws applied to the case of interfacial tension (see Eq. 12). This

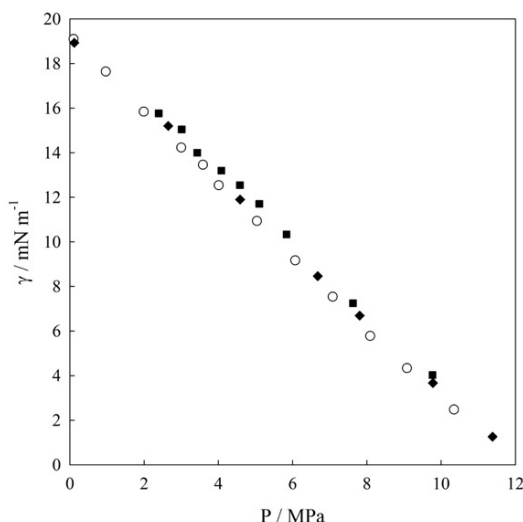


Figure 17. Interfacial tension for of $\text{CO}_2 + \text{n-C}_{10}\text{H}_{22}$ mixture at 344.3 K. O, Experimental [8]; ■, IK [8]; ♦, TA [9].

methodology is particular useful for the case of fluid with high of critical temperatures where the experimental determination is unattainable (e.g. in the cases where the fluids suffer a thermal decomposition). Some examples are the determination of the critical temperature of ionic liquids and longer alkanes over C_{16} .

6.5 Statistics and errors

An important aspect of reporting results is the evaluation of the errors associated with the calculations. For the case of interfacial properties, it is common to use block statistics where the information is averaged each n steps or cycles. In such a case, the production period is divided into n independent blocks. The statistical error is then deduced from the standard deviation of the average $\sigma/M^{1/2}$ where σ is the variance of the block averages and M is the number of blocks, usually a number close to 10. For further details, the reader is redirected to the Allen and Tildesley [15] and Frenkel and Smit [16] textbooks. Considering the advances in computer power (increased CPU and GPU speed, massive parallelization of codes, etc.), an alternative route to evaluate the statistics and deviation is to run the same MS a few times from different initial states then use the final results for each simulation to calculate the corresponding statistics, as if they were statistically different results.

Finally, it should be noted that several more advanced techniques are available for estimating the statistical errors in interfacial properties. One approach which is implemented in the GROMACS simulation software, and described in the appendix of Ref. [104], is to estimate the autocorrelation of the pressure tensor components and to use this information in constructing an optimal error estimate. Another technique

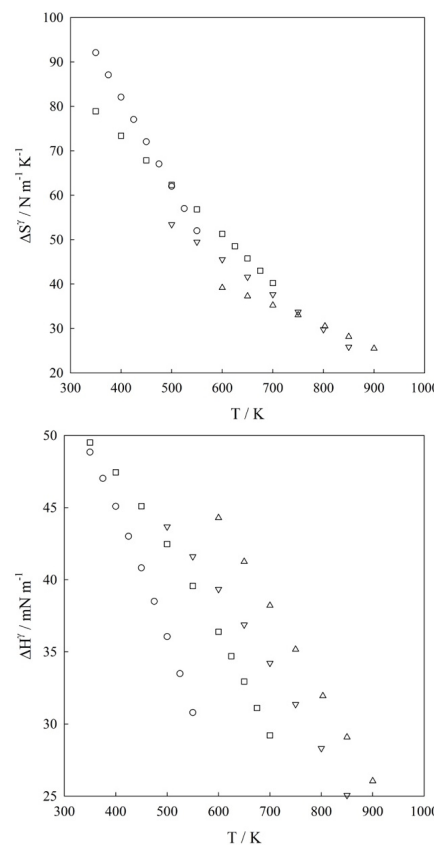


Figure 18. The surface entropy (S^γ) and surface enthalpy (H^γ) change as a function of temperature for selected n-alkanes. O, $\text{C}_{10}\text{H}_{22}$; □, $\text{C}_{20}\text{H}_{42}$; △, $\text{C}_{60}\text{H}_{122}$; ▽, $\text{C}_{100}\text{H}_{202}$. (adapted from Ref. [103])

which may be easier to implement is the so-called “jackknife” technique, illustrated in Fig. 19. In this approach, instead of dividing the production period into n blocks, one constructs a similar number of alternative blocks each of which comprise the entire data set *except for* the block in question. This falls under the more general topic of bootstrapping techniques, which are covered in statistics textbooks [105]. Finally, recent work by Rotenberg [106] has explored using the forces computed in molecular simulations to give reduced variance estimators.

7 Common Pitfalls

In this section, a summary of the most common pitfalls are presented as well as their impact in the final results.

7.1 Inappropriate initial density

A reasonable initial average of the expected liquid and vapor densities at the simulation temperature is required for a two-phase simulation. The choice of the initial density has an influence on the volume of each phase which will be present at equilibrium. If too few (too many) molecules are present in the simulation box, *i.e.* the global density is too low (high), the

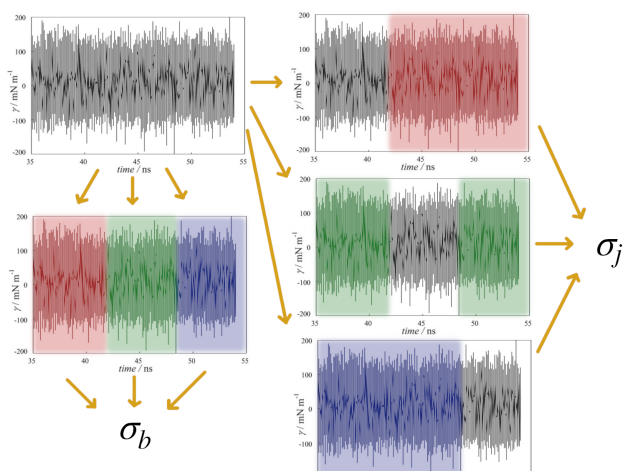


Figure 19. Illustration of block averages giving an error estimate σ_b (left) vs. the jackknife approach giving σ_j (right).

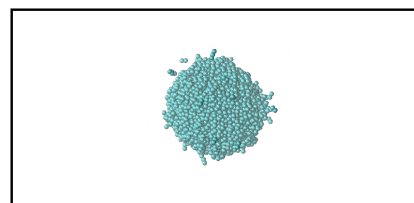
condensed (vapor) phase will not be able to span the short dimensions of the box, essentially condensing into a drop (bubble). This configuration (Fig. 20(a)) does not allow the calculation of interfacial tensions, as the heterogeneity of the system is incompatible with the assumptions made in Eq. 1.

A reasonably sized liquid slab (Fig. 20(c)) should be wide enough to comfortably host a bulk liquid region and its accompanying two interfaces. Too large of an initial density creates problems of a different kind, such as the possible lack of a coexisting vapor phase. The volume occupied by the vapor region must be larger than the liquid region, as the statistics in the former phases are inherently poorer. See Holcomb *et al.* [32] for further discussions relating to the use of inappropriate initial densities and the impact on the interfacial tension calculations.

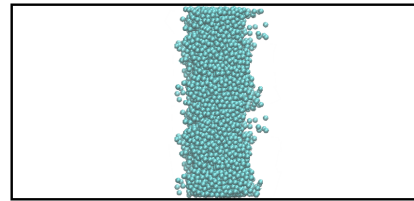
An associated error appears when the densities are chosen too close to the actual phase boundaries, hence giving rise to the possibility of metastable one-phase systems when otherwise a phase split is expected. *NVT* simulations artificially enhance the stability of liquid phases, by allowing the metastable states such as drops in a cylindrical or spherical shape to persist [65]. For further details concerning these metastable configurations, the reader is redirected to the recent review from Malijevsky and Jackson [27].

7.2 Selection of cutoff

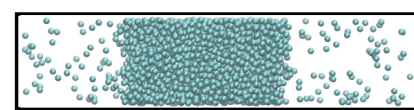
The value of the interfacial tension obtained from a force field is particularly susceptible to the choice of cutoff, as exemplified in Fig. 8. The most visible effects of choosing a low values of the cutoff are the underprediction of the bulk liquid and vapor densities. Lower values of the liquid density and higher values of vapor density directly impact the final value of the interfacial tension ($\gamma \simeq (\rho^L - \rho^V)^4$). A key point however



(a) Average density very low, no liquid slab



(b) Average density increased, but liquid slab too narrow



(c) Correct average density

Figure 20. Schematic illustration of common pitfalls in the initial density. (a) The overall density is too low and the condensed phase forms a droplet. (b) Increasing the density has removed the droplet. Now a slab spans the entire cell. However, the width of the liquid slab is too small and the interfacial regions play a significant role in the density profile. (c) A correct vapor-liquid ratio.

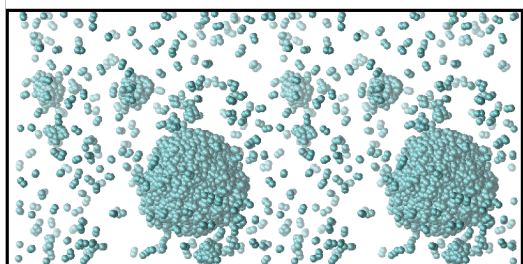
is to recognize that the parametrization of the force fields is performed for a given cutoff-radius. Hence the choice of the cutoff is generally not arbitrary, but dictated by the model employed. A related problem is associated with the choice of box dimensions; it is crucial to verify that the length of shortest side (L_x and L_y) be at least twice the cutoff radius.

7.3 Poor temperature control/choice

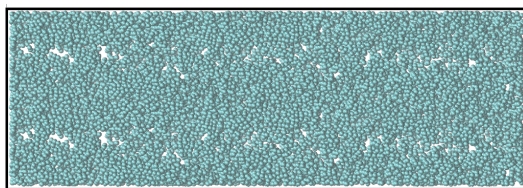
MS for interfacial properties of fluids are traditionally carried out in two ensembles: *NVT* and *NP_{zz}AT*, where the definition of the temperature is required. However, the temperature range needs to be selected very carefully to obtain trustworthy results of interfacial properties in fluid-fluid interfaces. At low temperatures, the MS can display cluster formation indicating the onset of a solid-like phase (see Fig. 21 (a)). At high temperatures (near to the critical state), the interfacial region will be very diffuse causing a poor definition of both the bulk densities and the interfacial region (see Fig. 21b). In order to avoid these effects, it is recommended to carry out MS at temperatures from $0.5 < T/T_c < 0.90$.

7.4 Insufficiently long simulation

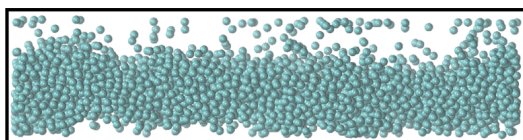
Based on the nature of the interfacial region, the MS needs to be run for longer simulation time (*i.e.*, steps or cycles) than homogeneous fluids to account for the longer diffusion times



(a) temperature close to the triple point



(b) temperature too close to critical state

Figure 21. Illustration of poor temperature choices**Figure 22.** Illustration of insufficient equilibration time

associated with phase rearrangement and with the elongated shape of the simulation box. As a general guideline, the simulation time for inhomogeneous fluids is three times the simulation time for equivalent homogenous ones. Speedups can be achieved by using a thermal quench first and then setting the thermostat to the selected simulation temperature [107]. Fig. 22 illustrates the case where insufficient equilibration time was used.

7.5 Bugs and humans

Our amazement at the speed in which modern computers can process data often blinds us from the obvious statement that the computers are not (yet) intelligent. Modern simulation codes will be composed of many thousands of lines of code, usually contributed by authors spanning lengths of space and time. Such collaboration is fruitful, but inevitably brings in the possibility of making mistakes. The corresponding number of coding errors (bugs) in a modern MS code is estimated to be in the upper 100's [108], even after extensive testing. Many of these bugs will be inconsequential to a simulation, but some might eventually creep into the results. More frequently however, human errors and faulty implementations are the cause of fatal errors [78]. In either case, it is important to validate in detail an existing calculation (as provided in this manuscript) and to ensure reproducibility and to minimize

the pernicious effect of bugs and humans.

8 Conclusions

Molecular simulation (MS) of interfacial properties of pure fluids and fluid mixtures can be carried out by using Molecular Dynamics or Monte Carlo schemes. However, the design of the molecular simulation and the route to evaluate the interfacial properties plays a central role to obtain meaningful results. This work provides a detailed guide to the design and analysis of molecular simulations of inhomogeneous fluids to obtain the most important interfacial properties of fluids.

For biphasic fluid systems (vapor-liquid and liquid-liquid), we suggest to design the simulation box dimension using the average of the bulk phases at the selected temperature (or at the lower value of temperature to be simulated) with a total number of particles ranging from 5000 to 8000 sites, which can be described as united atoms (UA) and coarse-grained atoms (CG). The ideal simulation box is a parallelepiped cell with $L_x = L_y > 10 \sigma_{\text{max}}$ (the larger molecular diameter) and $L_z = 3$ to $10 L_x$. The initial configuration of the molecules in the simulation box should be assigned using their spatial positions in a solidlike configuration without velocities nor forces. This initial configuration should be first simulated at high temperature (above the critical state) to homogenize the system. After a few steps, the final configuration is quenched and used as the initial configuration to carry out the MS at the desired temperature.

In order to reach an equilibrium state, we suggest using either the *NVT* or *NP_{zz}AT* ensembles, where it is necessary to use a thermostat to fix the temperature and/or a barostat to fix the pressure. A very common choice is the Nosé-Hoover, which includes constants (τ) to control the MS conditions. The range of these constant are τ_T are 0.5 to 2 ps, and τ_P are 0.2 to 1 ps, for temperature and pressure respectively. The simulation length for inhomogeneous fluids needs to be larger than for homogeneous fluids. For the case of MD, it is advised to use 10 to 15 ns for equilibration stage, and 30 ns for the production state. For the case of mixtures, the system should be equilibrated for 70 to 80 ns, and then another 150 ns for production. During the production stage, it is advised to use block statistics to collect the numerical results.

The actual calculation of interfacial tensions should be performed by dividing the simulation box in n slabs ($n \approx 250$ to 500) along the z-direction. Within each slab, the density and the pressure tensor (e.g., using the Irving-Kirkwood formulation) and the results averaged on a per-slab basis. These results will be used to calculate other interfacial properties such as the relative Gibbs adsorption isotherm, surface entropy, and surface enthalpy change and the interfacial tension.

Besides provided general recommendations for advanta-

geous methods, this work also includes worked-out examples and input files required to carry out the corresponding simulations to reproduce selected results presented here.

Potentially Conflicting Interests

The authors declare no conflicting interests.

Funding Information

A.M. acknowledges funding from Fondecyt (Chile) through Grant 1190107. E.A.M. acknowledges funding from the Engineering and Physical Sciences Research Council to the Molecular Systems Engineering group through Grant Nos. EP/E016340, EP/I018212 and EP/J014958 and EP/R013152. Å.E. acknowledges funding from the Research Council of Norway (RCN) through the CLIMIT program (254813/E20), and through the HYVA project which is part of the Strategic Institute Programme of SINTEF Energy Research funded through the Basic Research Funding scheme of the Research Council of Norway.

Author Information

ORCID:

Erich A. Müller: [0000-0002-1513-6686](https://orcid.org/0000-0002-1513-6686)

Åsmund Ervik: [0000-0003-1073-887X](https://orcid.org/0000-0003-1073-887X)

Andres Mejía: [0000-0001-7238-6633](https://orcid.org/0000-0001-7238-6633)

Appendix A Checklist

The recommendations of this manuscript are summarized in the checklist provided on the next page.

Supplementary Information: Attached code examples

Some example codes are attached to this manuscript at <https://github.com/asmunder/BPIPMDs>. These can be used for computing the interfacial properties of three systems: coarse-grained CO₂, coarse-grained decane, and finally a mixture of these. The example codes are provided for DL_POLY, HOOMD, and LAMMPS.

SETUP

Steps for setup the initial conditions

- Select the *NVT* ensemble
- Select an appropriate total number of particles, N_T ($N_T = N^L + N^V$; $N^L \approx 2000$ to 5000 ; $N^V \approx 1000$ to 2000). For mixtures, check to see if there are enough molecules of each type to satisfy the expected compositions in each phase. [See Example 1 and Example 2.](#)
- Choose a global density of the pure fluid or fluid mixture at T_{ref} (i.e., $\rho = (\rho^L + \rho^V)/2$). [See discussion around Fig. 20.](#)
- Calculate the simulation cell parameters ($V = N_T / \rho = L_x L_y L_z$; $L_x = L_y > 10 \sigma_{\max}$; $L_z \approx 3$ to $10 L_x$). [See Example 2.](#)
- Choose a force field: UA or CG. [See Sec. 5.3.](#)
- Select a cutoff compatible with the force field, otherwise choose $r_c \geq 6 \sigma_{\max}$. Verify that $r_c^{\max} = L_x / 2$. [See Sec. 5.4.](#)
- Select a thermostat (e.g. Nosé-Hoover or better) with an appropriate constant ($\tau_T \approx 0.5$ to 1 ps). [See Sec. 5.2.](#) If using Verlet radii, choose $delr = 1.5 \sigma_{\max}$
- Set total Simulation Steps ($SS \approx 50000$ to 100000).
- Set a time step ($\Delta t \approx 0.01$ to 0.003 ps)
- Run MS at high temperature ($T_H \gg T_C$) to generate an initial configuration for the quench. [See Sec. 4.](#)

PRODUCTION RUN

Steps for running simulation at production conditions, after setup

- Set simulation ensemble: *NVT* or *NP_{zz}AT*. [See Sec. 5.1.](#)
- Set simulation temperature T_s ($0.5 < T/T_c < 0.90$)
- Set simulation pressure P_{zz} (only for *NP_{zz}AT*)
- Select a thermostat as before, and (only for *NP_{zz}AT*) a barostat with an appropriate constant $\tau_p \approx 0.5$ to 1 ps, i.e. a barostat that maintains the desired P_{zz} by scaling only the z-dimension of the box. [See Sec. 5.2.](#)
- Set total Simulation Steps ($SS \approx 20 \times 10^6$ for pure fluids; 40×10^6 for fluids mixtures) of which the first third should be discarded as equilibration steps. [See Sec. 5.5.](#)
- Decide strategy for statistics, visualization, printing of configurations to disk (frequency to save) and post-processing (if not included in main program). [See Sec. 6.](#)

References

- [1] Evans MJB. Measurement of surface and interfacial tension. In: Weir RD, de Loos TW, editors. *Measurement of the thermodynamic properties of multiple phases*, vol. VII Amsterdam: Elsevier; 2006.
- [2] Hansen JP, McDonald IR. Theory of simple liquids: with applications to soft matter. Academic Press; 2013.
- [3] Evans R, Oettel M, Roth R, Kahl G. New developments in classical density functional theory. *Journal of Physics: Condensed Matter*. 2016; 28:240401.
- [4] Wu J. Density functional theory for chemical engineering: From capillarity to soft materials. *AIChE journal*. 2006; 52(3):1169–1193.
- [5] Evans R. Density functionals in the theory of nonuniform fluids. In: Henderson D, editor. *Fundamentals of inhomogeneous fluids* Marcel Dekker, New York: Henderson; 1992.
- [6] Rowlinson JS, Widom B. Molecular theory of capillarity. Oxford: Clarendon; 1982.
- [7] Davis HT, Scriven LE. Stress and structure in fluid interfaces. *Adv Chem Phys*. 1982; 49:357–454. <https://doi.org/10.1002/9780470142691.ch6>.
- [8] Mejía A, Cartes M, Segura H, Müller EA. Use of equations of state and coarse grained simulations to complement experiments: describing the interfacial properties of carbon dioxide + decane and carbon dioxide + eicosane mixtures. *J Chem Eng Data*. 2014; 59:2928–2941. <https://doi.org/10.1021/je5000764>.
- [9] Müller EA, Mejía A. Interfacial properties of selected binary mixtures containing n-alkanes. *Fluid Phase Equilibria*. 2009; 282:68–81. <https://doi.org/10.1016/j.fluid.2009.04.022>.
- [10] Mejía A, Pàmies JC, Duque D, Segura H, Vega LF. Phase and interface behavior in Type I and Type V Lennard-Jones mixtures: Theory and Simulations. *J Chem Phys*. 2005; 123:034505 – 034515. <https://doi.org/10.1063/1.1955529>.
- [11] Müller EA, Mejía A. Extension of the SAFT-VR Mie EoS to model homonuclear rings and its parametrization based on the principle of corresponding states. *Langmuir*. 2017; 33(42):11518–11529.
- [12] Garrido JM, Mejía A, Pineiro MM, Blas FJ, Müller EA. Interfacial tensions of industrial fluids from a molecular-based square gradient theory. *AIChE Journal*. 2016; 62(5):1781–1794.
- [13] Cárdenas H, Mejía A. Phase behaviour and interfacial properties of ternary system CO₂ + n-butane + n-decane: coarse-grained theoretical modelling and molecular simulations. *Molecular Physics*. 2016; 114(18):2627–2640.
- [14] Dukhin SS, Kretzschmar G, Miller B. Dynamics of Adsorption at Liquid Interfaces. Amsterdam: Elsevier; 1995.
- [15] Allen MP, Tildesley DJ. Computer Simulation of Liquids. 2nd ed. Oxford: Oxford University Press; 2017.
- [16] Frenkel D, Smit B. Understanding Molecular Simulation: From Algorithms to Applications. 2nd ed. Amsterdam: Elsevier; 2002.
- [17] Various. Computing power revolution and new algorithms: GP-GPUs, clouds and more: general discussion. *Faraday Discuss*. 2014; 169:379–401. <https://doi.org/10.1039/c4fd90021a>.
- [18] Liu KS. Phase separation of Lennard-Jones systems: A film in equilibrium with vapor. *J Chem Phys*. 1974; 60:4226–4230. <https://doi.org/10.1063/1.1680892>.
- [19] Algabe J, Míguez JM, Gómez-Álvarez P, Mejía A, Blas FJ. Preferential Orientations and Anomalous Interfacial Tensions in Aqueous Solutions of Alcohols. *The Journal of Physical Chemistry B*. 2020; 124(38):8388–8401.
- [20] Müller EA, Mejía A. Resolving discrepancies in the measurements of the interfacial tension for the CO₂+H₂O mixture by computer simulation. *The journal of physical chemistry letters*. 2014; 5(7):1267–1271.
- [21] Herdes C, Ervik A, Mejía A, Müller EA. Prediction of the water/oil interfacial tension from molecular simulations using the coarse-grained SAFT- γ Mie force field. *Fluid Phase Equilibria*. 2018; 476:9–15. <https://doi.org/10.1016/j.fluid.2017.06.016>.
- [22] Chen JL, Xue B, Harwood DB, Chen QP, Peters CJ, Siepmann JL. A Monte Carlo simulation study of the interfacial tension for water/oil mixtures at elevated temperatures and pressures: Water/n-dodecane, water/toluene, and water/(n-dodecane + toluene). *Fluid Phase Equilibria*. 2018; 476:16–24. <https://doi.org/10.1016/j.fluid.2017.06.015>.
- [23] Papavasileiou KD, Mourtos OA, Economou IG. Predictions of water/oil interfacial tension at elevated temperatures and pressures: A molecular dynamics simulation study with biomolecular force fields. *Fluid Phase Equilibria*. 2018; 476:30 – 38. <https://doi.org/https://doi.org/10.1016/j.fluid.2017.05.004>.
- [24] Alonso G, Chaparro G, Cartes M, Müller EA, Mejía A. Probing the interfacial behavior of Type IIIa binary mixtures along the three-phase line employing molecular thermodynamics. *Molecules*. 2020; 25(7):1499.
- [25] Stephan S, Hasse H. Interfacial properties of binary mixtures of simple fluids and their relation to the phase diagram. *Physical Chemistry Chemical Physics*. 2020; 22:12544–12564. <https://doi.org/10.1039/D0CP01411G>.
- [26] Sampayo JG, Malijevský A, Müller EA, de Miguel E, Jackson G. Evidence for the role of fluctuations in the thermodynamics of nanoscale drops and the implications in computations of the surface tension. *J Chem Phys*. 2010; 132:14110. <https://doi.org/10.1063/1.3376612>.
- [27] Malijevský A, Jackson G. A perspective on the interfacial properties of nanoscopic liquid drops. *Journal of Physics: Condensed Matter*. 2012; 24(46):464121.
- [28] Wilhelmsen Ø, Bedeaux D, Reguera D. Tolman length and rigidity constants of the Lennard-Jones fluid. *The Journal of Chemical Physics*. 2015; 142(6):064706. <https://doi.org/10.1063/1.4907588>.
- [29] Min SH, Berkowitz ML. Bubbles in water under stretch-induced cavitation. *The Journal of Chemical Physics*. 2019; 150(5):054501. <https://doi.org/10.1063/1.5079735>.

- [30] **Gray CG**, Gubbins KE, Joslin CG. Theory of Molecular Fluids: Vol. 2: Applications. New York: Oxford University Press; 2011.
- [31] **Ghoufi A**, Malfreyt P, Tildesley DJ. Computer modelling of the surface tension of the gas-liquid and liquid-liquid interface. *Chem Soc Rev.* 2016; 45:1387–1409. <http://dx.doi.org/10.1039/C5CS00736D>.
- [32] **Holcomb CD**, Clancy P, Zollweg JA. A critical study of the simulation of the liquid-vapour interface of a Lennard-Jones fluid. *Mol Phys.* 1993; 78:437–459. <https://doi.org/10.1080/00268979300100321>.
- [33] **Gloor GJ**, Jackson G, Blas FJ, de Miguel E. Test-area simulation method for the direct determination of the interfacial tension of systems with continuous or discontinuous potentials. *J Chem Phys.* 2005; 123:134703–1–134703–19. <https://doi.org/10.1063/1.2038827>.
- [34] **Zhang Y**, Feller SE, Brooks BR, Pastor RW. Computer simulation of liquid/liquid interfaces. I. Theory and application to octane/water. *J Chem Phys.* 1995; 103:10252–10266. <https://doi.org/10.1063/1.46992>.
- [35] **Ervik Å**, Serratos GJ, Müller EA. raaSAFT: A framework enabling coarse-grained molecular dynamics simulations based on the SAFT- γ Mie force field. *Computer Physics Communications.* 2017; 212:161–179.
- [36] **Sega M**, Hantal G, Fábián B, Jedlovszky P. Pytim: A python package for the interfacial analysis of molecular simulations. *Journal of Computational Chemistry.* 2018; 39(25):2118–2125.
- [37] **Walton JPRB**, Tildesley DJ, Rowlinson JS, Henderson JR. The pressure tensor at the planar surface of a liquid. *Mol Phys.* 1983; 48:1357–1368. <https://doi.org/10.1080/00268978300100971>.
- [38] **Chapela GA**, Saville G, Thompson SM, Rowlinson JS. Computer simulation of a gas-liquid surface. Part 1. *Faraday Trans.* 1977; 2(73):1133–1144. <https://doi.org/http://dx.doi.org/10.1039/F29777301133>.
- [39] **Trokhymchuk A**, Alejandre J. Computer simulations of liquid/vapor interface in Lennard-Jones fluids: Some questions and answers. *J Chem Phys.* 1999; 111:8510–8523. <https://doi.org/10.1063/1.480192>.
- [40] **Mecke M**, Winkelmann J, Fischer J. Molecular dynamics simulation of the liquid-vapor interface: The Lennard-Jones fluid. *J Chem Phys.* 1997; 107:9264–9240. <https://doi.org/10.1063/1.475217>.
- [41] **Mecke M**, Winkelmann J, Fischer J. Molecular dynamics simulation of the liquid-vapor interface: Binary mixtures of Lennard-Jones fluids. *J Chem Phys.* 1999; 110:1188–1194. <https://doi.org/10.1063/1.478160>.
- [42] **Duque D**, Vega L. Some issues on the calculation of interfacial properties by molecular simulation. *J Chem Phys.* 2004; 121:8611–8617. <https://doi.org/10.1063/1.1802672>.
- [43] **Errington JR**, Kofke DA. Calculation of surface tension via area sampling. *J Chem Phys.* 2007; 127:174709–1 – 174709–12. <https://doi.org/10.1063/1.2795698>.
- [44] **Stephan S**, Langenbach H, Hasse H. Interfacial properties of binary Lennard-Jones mixtures by molecular simulation and density gradient theory. *J Chem Phys.* 2019; 150(174704). <https://doi.org/10.1063/1.5093603>.
- [45] **Braun E**, Gilmer J, Mayes HB, Mobley DL, Monroe JL, Prasad S, Zuckerman DM. Best Practices for Foundations in Molecular Simulations [Article v1.0]. *Living Journal of Computational Molecular Science.* 2018; 1(1):5957. <https://doi.org/10.33011/livecoms.1.1.5957>.
- [46] **Bopp PA**, Hawlicka E, Fritzsche S. The Hitchhiker's guide to molecular dynamics. *ChemTexts.* 2018; 4(1):2.
- [47] **Grossfield A**, Patrone PN, Roe DR, Schultz AJ, Siderius D, Zuckerman DM. Best Practices for Quantification of Uncertainty and Sampling Quality in Molecular Simulations [Article v1.0]. *Living Journal of Computational Molecular Science.* 2018; 1(1):5067. <https://doi.org/10.33011/livecoms.1.1.5067>.
- [48] Wikipedia: comparison of MS software; https://en.wikipedia.org/wiki/Comparison_of_software_for_molecular_mechanics_modeling, last accessed April 2020.
- [49] Avogadro; <https://avogadro.cc>, last accessed April 2020.
- [50] xmgrace; <http://plasma-gate.weizmann.ac.il/Grace/>, last accessed April 2020.
- [51] VMD: Visual Molecular Dynamics; <https://www.ks.uiuc.edu/Research/vmd/>, last accessed April 2020.
- [52] OVITO; <https://www.ovito.org/>, last accessed April 2020.
- [53] PyMol; <https://pymol.org/2/>, last accessed April 2020.
- [54] **Lemmon EW**, Huber ML, McLinden MO, NIST Standard Reference Database 23: Reference Fluid Thermodynamic and Transport Properties - REFPROP, Version 9.1; 2013. <https://webbook.nist.gov/chemistry/>, standard Reference Data Program, National Institute of Standards and Technology.
- [55] **Stephan S**, Hasse H. Enrichment at vapour-liquid interfaces of mixtures: establishing a link between nanoscopic and macroscopic properties. *International Reviews in Physical Chemistry.* 2020; 39(3):319–349.
- [56] **Garrido JM**, Piñeiro MM, Mejía A, Blas FJ. Understanding the interfacial behavior in isopycnic Lennard-Jones mixtures by computer simulations. *Physical Chemistry Chemical Physics.* 2016; 18(2):1114–1124.
- [57] **Bresme F**, Chacón E, Tarazona P. Molecular dynamics investigation of the intrinsic structure of water-fluid interfaces via the intrinsic sampling method. *Physical Chemistry Chemical Physics.* 2008; 10(32):4704–4715.
- [58] **Bresme F**, Chacón E, Tarazona P, Tay K. Intrinsic structure of hydrophobic surfaces: The oil-water interface. *Physical Review Letters.* 2008; 101(5):056102.
- [59] **Hulshof H**. The direct deduction of the capillary constant σ as a surface-tension. In: *Proc. Sect. Sci. Konink. Akad. Weten. Amsterdam;* 1901. p. 389–398. See also *Ann. Physik* 309 (1):165–186.

- [60] **Binder K.** Monte Carlo calculation of the surface tension for two- and three-dimensional lattice-gas models. *Phys Rev A.* 1982; 25:1699–1709. <https://doi.org/10.1103/PhysRevA.25.1699>.
- [61] **Errington JR.** Evaluating surface tension using grand-canonical transition-matrix Monte Carlo simulation and finite-size scaling. *Phys Rev E.* 2003; 67(012102). <https://doi.org/10.1103/PhysRevE.67.012102>.
- [62] **Schrader M**, Virnau P, Winter D, Zykova-Timan T, Binder K. Methods to extract interfacial free energies of flat and curved interfaces from computer simulations. *Eur Phys J Special Topics.* 2009; 177:103–127. <https://doi.org/10.1140/epjst/e2009-01170-y>.
- [63] **Telo da Gama MM**, Evans R. The structure and surface tension of the liquid-vapour interface near the upper critical end point of a binary mixture of Lennard-Jones fluids: I. The two phase region. *Molecular Physics.* 1983; 48(2):229–250.
- [64] **Defay R**, Bellemans A, Prigogine I. Surface tension and adsorption. Longmans; 1966.
- [65] **Lau GV**, Ford JJ, Hunt PA, Müller EA, Jackson G. Surface thermodynamics of planar, cylindrical, and spherical vapour-liquid interfaces of water. *J Chem Phys.* 2015; 142:114701. <https://doi.org/10.1063/1.4913371>.
- [66] **Gonzalez-Melchor M**, Orea P, López-Lemus J, Bresme F, Alejandro J. Stress anisotropy induced by periodic boundary conditions. *J Chem Phys.* 2005; 122:094503 1–8. <https://doi.org/10.1063/1.1854625>.
- [67] **Orea P**, López-Lemus J, Alejandro J. Oscillatory surface tension due to finite-size effects. *J Chem Phys.* 2005; 123(11470):14702–6. <https://doi.org/10.1063/1.2018640>.
- [68] **Janecek J.** Effect of the interfacial area on the equilibrium properties of Lennard-Jones fluid. *J Chem Phys.* 2009; 131(12451):24513–9. <https://doi.org/10.1063/1.3238550>.
- [69] **Avendaño C**, Lafitte T, Galindo A, Adjiman CS, Jackson G, Müller EA. SAFT- γ force field for the simulation of molecular fluids. 1. A single-site coarse grained model of carbon dioxide. *J Phys Chem B.* 2011; 115:11154–11169. <https://doi.org/10.1021/jp204908d>.
- [70] **Martínez-Veracoechea F**, Müller EA. Temperature-quench molecular dynamics simulations for fluid phase equilibria. *Molecular Simulation.* 2005; 31:33 – 43. <https://doi.org/10.1080/08927020412331298991>.
- [71] **Shaver RD**, Robinson Jr RL, Kam G. An automated apparatus for equilibrium phase compositions, densities, and interfacial tensions: data for carbon dioxide + decane. *Fluid Phase Equilibria.* 2001; 179:43 – 66. [https://doi.org/10.1016/S0378-3812\(00\)00475-1](https://doi.org/10.1016/S0378-3812(00)00475-1).
- [72] **Kunz O**, Wagner W. The GERG-2008 wide-range equation of state for natural gases and other mixtures: an expansion of GERG-2004. *J Chem Eng Data.* 2012; 57:3032–3091. <https://doi.org/10.1021/je300655b>.
- [73] **Lafitte T**, Apostolakou A, Avendaño C, Galindo A, Adjiman CS, Müller EA, Jackson G. Accurate statistical associating fluid theory for chain molecules formed from Mie segments. *J Chem Phys.* 2013; 139(15):54504–37. <https://doi.org/10.1063/1.4819786>.
- [74] **McCabe C**, Galindo A. SAFT associating fluids and fluid mixtures. *Applied Thermodynamics of Fluids.* 2010; p. 215–279.
- [75] **Hoover WG.** Canonical dynamics: equilibrium phase-space distributions. *Phys Rev A.* 1985; 31:1695–1697. <https://doi.org/10.1103/PhysRevA.31.1695>.
- [76] **Martyna GJ**, Klein ML, Tuckerman M. Nosé - Hoover chains: the canonical ensemble via continuous dynamics. *J Chem Phys.* 1992; 97:2635–2643. <https://doi.org/10.1063/1.463940>.
- [77] **Shirts MR.** Simple quantitative tests to validate sampling from thermodynamic ensembles. *J Chem Theory Comput.* 2013; 9:909–926. <https://doi.org/10.1021/ct300688p>.
- [78] **Wong-ekkabut J**, Karttunen M. The good, the bad and the user in soft matter simulations. *BBA - Biomembranes.* 2016; 1858:2529–2538. <https://doi.org/10.1016/j.bbamem.2016.02.004>.
- [79] **Berendsen HJC**, Postma JPM, van Gunsteren WF, Di Nola A, Haak JR. Molecular dynamics with coupling to an external bath. *J Chem Phys.* 1984; 81:3684–3690. <https://doi.org/http://dx.doi.org/10.1063/1.448118>.
- [80] **Braun E**, Moosavi SM, Smit B. Anomalous effects of velocity rescaling algorithms: the flying ice cube effect revisited. *Journal of Chemical Theory and Computation.* 2018; 14(10):5262–5272.
- [81] **Tuckerman ME.** Statistical Mechanics: Theory and Molecular Simulation. Oxford, England: Oxford University Press; 2010.
- [82] **Leach AR.** Molecular modelling: principles and applications. Pearson Education; 2001.
- [83] **Jiménez-Serratos G**, Vega C, Gil-Villegas A. Evaluation of the pressure tensor and surface tension for molecular fluids with discontinuous potentials using the volume perturbation method. *The Journal of Chemical Physics.* 2012; 137(20):204104. <https://doi.org/10.1063/1.4767375>.
- [84] **Müller EA**, Jackson G. Force-field parameters from the SAFT- γ equation of state for use in coarse-grained molecular simulations. *Annu Rev Chem Biomol Eng.* 2014; 5:405–427. <https://doi.org/10.1146/annurev-chembioeng-061312-103314>.
- [85] **Blas FJ**, MacDowell LG, de Miguel E, Jackson G. Vapor-liquid interfacial properties of fully flexible Lennard-Jones chains. *J Chem Phys.* 2008; 129:144703–1 – 144703–9. <https://doi.org/10.1063/1.2989115>.
- [86] **Lotfi A**, Vrabec J, Fischer J. Orthobaric Densities from Simulations of the Liquid Vapour Interface. *Molecular Simulation.* 1990; 5:233–243. <https://doi.org/10.1080/0892702900822133>.
- [87] **Janeček J.** Long Range Corrections in Inhomogeneous Simulations. *J Phys Chem B.* 2006; 110:6264 – 6269. <https://doi.org/10.1021/jp056344z>.

- [88] Siperstein F, Myers AL, Talu O. Long range corrections for computer simulations of adsorption. *Mol Phys.* 2002; 100:2025–2030. <https://doi.org/10.1080/00268970110109916>.
- [89] Lishchuk SV, Fischer J. Long range corrections in liquid-vapor interface simulations. *J Chem Phys.* 2018; 149:091102. <https://doi.org/10.1063/1.5048925>.
- [90] Martínez-Ruiz FJ, Blas F, Mendiboure B, Moreno-Ventas Bravo A. Effect of dispersive long-range corrections to the pressure tensor: The vapour-liquid interfacial properties of the Lennard-Jones system revisited. *The Journal of Chemical Physics.* 2014; 141(18):184701.
- [91] Ibergay C, Ghoufi A, Goujon F, Ungerer P, Boutin A, Rousseau B, Malfreyt P. Molecular simulations of the n-alkane liquid-vapor interface: Interfacial properties and their long range corrections. *Physical Review E.* 2007; 75(5):051602.
- [92] Ewald PP. Die Berechnung optischer und elektrostatischer Gitterpotentiale. *Ann Phys.* 1921; 369:253–287. <https://doi.org/10.1002/andp.19213690304>.
- [93] Barker JA, Watts RO. Monte Carlo studies of the dielectric properties of water-like models. *Mol Phys.* 1973; 26:789–792. <https://doi:10.1080/00268977300102101>.
- [94] Watts RO. Monte Carlo studies of liquid water. *Mol Phys.* 1974; 28:1069–1083. <https://doi.org/10.1080/00268977400102381>.
- [95] Darden TA, York DM, Pedersen LG. Particle mesh Ewald: An N-log(N) method for Ewald sums in large systems. *J Chem Phys.* 1993; 98:10089–10092. <https://doi.org/10.1063/1.464397>.
- [96] Wolf D, Kebinski P, Phillipot SR, Eggebrecht J. Exact method for the simulation of Coulombic systems by spherically truncated, pairwise r^{-1} summation. *J Chem Phys.* 1999; 110:8254–8282. <https://doi.org/10.1063/1.478738>.
- [97] Fischer NM, van Maaren PJ, Ditz JC, Yildirim A, van der Spoel D. Properties of Organic Liquids when Simulated with Long-Range Lennard-Jones Interactions. *Journal of Chemical Theory and Computation.* 2015; 11(7):2938–2944. <https://doi.org/10.1021/acs.jctc.5b00190>.
- [98] Fincham D. Choice of timestep in molecular dynamics simulation. *Computer Physics Communications.* 1986; 40(2-3):263–269.
- [99] Kim S. Issues on the choice of a proper time step in molecular dynamics. *Physics Procedia.* 2014; 53:60–62.
- [100] Irving JH, Kirkwood JG. The statistical mechanical theory of transport processes. IV. The equations of hydrodynamics. *J Chem Phys.* 1950; 18:817–829. <https://doi.org/10.1063/1.1747782>.
- [101] Harasima A. Molecular Theory of Surface Tension. *Advances in Chemical Physics.* 1957; 1:203–237. <https://doi.org/10.1002/9780470143476.ch7>.
- [102] Long Y, Palmer JC, Coasne B, Śliwińska Bartkowiak M, Jackson G, Müller EA, Gubbins KE. On the molecular origin of high-pressure effects in nanoconfinement: The role of surface chemistry and roughness. *J Chem Phys.* 2013; 139:144701. <https://doi.org/10.1063/1.4824125>.
- [103] Müller EA, Mejía A. Comparison of United-Atom potentials for the simulation of vapor-liquid equilibria and interfacial properties of long-chain n-alkanes up to n-C100. *J Phys Chem B.* 2011; 115:12822–12834. <https://doi.org/10.1021/jp203236q>.
- [104] Hess B. Determining the shear viscosity of model liquids from molecular dynamics simulations. *J Chem Phys.* 2002; 116. <https://doi.org/10.1063/1.1421362>.
- [105] Efron B. The jackknife, the bootstrap, and other resampling plans. Philadelphia: SIAM; 1982.
- [106] Rotenberg B. Use the force! Reduced variance estimators for densities, radial distribution functions, and local mobilities in molecular simulations. *The Journal of Chemical Physics.* 2020; 153(15):150902.
- [107] Gelb L, Müller EA. Location of phase equilibria by temperature-quench molecular dynamics simulations. *Fluid Phase Equilibria.* 2002; 203:1–14. [https://doi.org/10.1016/S0378-3812\(02\)00174-7](https://doi.org/10.1016/S0378-3812(02)00174-7).
- [108] Schappals M, Mecklenfeld A, Kröger L, Botan V, Köster A, Stephan S, García Ej, Rutkai G, Raabe G, Klein P, Leonhard K, Glass CW, Lenhard J, Vrabec J, Hasse H. Round Robin Study: Molecular Simulation of Thermodynamic Properties from Models with Internal Degrees of Freedom. *J Chem Theory Comput.* 2017; 13:4270–4280. <https://doi.org/10.1021/acs.jctc.7b00489>.